Universität Zürich[UZH]

University of Zürich

Calibration data analysis for LEGEND-200

Bachelor Thesis

Author
Esteban Tapia Peñas
Supervisors
Prof. Dr. Laura Baudis
Dr. Pin-Jung Chiu

June 2024

Contents

Introduction **3**

1 Theory **4**
1.1 The Standard Model of particle physics and nuclear decays 4
1.2 Neutrinoless Double-β Decay 7

2 The LEGEND Experiment **9**
2.1 Experimental setup of LEGEND-200 9
2.2 Pulse Shape Discrimination 13
2.3 Calibration of LEGEND-200 14
2.3.1 Energy scale and resolution 15
2.3.2 Calibration procedure 16
2.3.3 Calibration source 17

3 Data Analysis – Calibration in the low-energy regime **20**
3.1 Coincident events in nearby detectors to look for possible low-energy events 21
3.1.1 Coincident events in two nearby detectors 22
3.1.2 Energy correlation for two detectors 27
3.2 New low-energy peaks for calibration of HPGe detectors 30

4 Results **34**

5 Conclusion and Outlook **39**

Appendix A **41**

Appendix A **41**
2D histograms 41

Appendix B **42**

Appendix B **42**
List of abbreviations 43

Abstract

The LEGEND experiment deploys high-purity germanium (HPGe) detectors enriched in the target isotope ^{76}Ge by up to 90%, in an active liquid argon shield to detect the neutrinoless double beta ($0\nu\beta\beta$) decay, a process generating two matter particles without the emission of any antimatter. In this work, the analyses of the calibration data for the LEGEND-200 experiment are addressed, with the aim of calibrating the 101 HPGe detectors used for this experiment. In the search for the monochromatic peak as the signature of $0\nu\beta\beta$ decay a stable energy scale and an excellent energy resolution around the Q-value of the decay ($Q_{\beta\beta}$ = 2039.061(7) keV for ^{76}Ge) are essential. Meticulous calibration procedures and data analysis techniques are employed to ensure the accuracy and reliability of these detectors, which are crucial for the search for the $0\nu\beta\beta$ decay in ^{76}Ge.

This work builds upon established calibration methodologies used in the GERDA and Majorana experiments, extending the calibrated energy range from 50 keV to 583 keV, an energy range that is not considered in the regular calibration procedure of the LEGEND-200 experiment. Three investigations were conducted using LEGEND-200 calibration data. An analysis in the energy range from 50 keV to 230 keV revealed the presence of two distinct lines at 74.815 keV and 77.107 keV emerging in the two-dimensional energy histogram, indicating a complete energy deposition of individual photons. Both photons are attributed to emissions from the ^{212}Pb isotope. An energy correlation analysis across the entire detector range (50 keV - 2.6 MeV) successfully identified anti-diagonal lines at 583 keV and 2.6 MeV indicative of partial energy depositions. Finally, the potential of including the newly identified peaks in the standard calibration procedure was explored. While the inclusion offered minimal improvement in detector resolution, the investigation highlights the continued importance of precise calibration in the 50 keV to 583 keV range relevant to future LEGEND-200 endeavors beyond the search for $0\nu\beta\beta$ decay. As a future direction, this thesis proposes an investigation into the efficacy of linear versus quadratic calibration curves to further refine the calibration protocols for the LEGEND-200 experiment.

Introduction

In the pursuit of advancing our understanding of fundamental particles and their interactions, modern experimental physics endeavors, such as the LEGEND-200 experiment, play a central role. The LEGEND-200 experiment is dedicated to probe neutrinoless double-beta decay in ^{76}Ge and represents a cornerstone of scientific exploration of exotic nuclear processes. Within this context, the precise energy calibration of detectors emerges as a crucial aspect, ensuring the accuracy and reliability of the energy scale and the resolution of the HPGe detectors. This thesis seeks to contribute to the ongoing calibration efforts within the LEGEND-200 experiment by digging into the analysis of calibration data with a specific focus on incorporating low-energy peaks that have not been utilized in the current standard calibration routine. By exploiting features of conventional energy peaks, particularly those arising from possible coincident events in nearby detectors, we aim to refine the calibration process and enhance the performance of the detectors. Crucial for this investigation is the energy of the γ peaks, since it need to be inside an energy range, where the cross section for Compton scattering is sufficiently high.

This thesis consists of five chapters. In chapter 1, a concise overview of particle physics is presented, covering the three primary types of nuclear decays and introducing the concept of neutrinoless double-beta decay. Chapter 2 provides an overview of the LEGEND experiment, including details about the experimental setup, the high purity germanium detectors, and the relevant steps for the calibration of such detectors; the importance of calibration is underlined in this section. This is followed by the central focus of the thesis, chapter 3, where calibration data from LEGEND-200 is examined, with particular attention paid to the low-energy region. Next, the results of the studies are presented in chapter 4, and the concluding chapter 5 summarizes the work presented throughout this thesis.

1 Theory

Astroparticle physics is a branch of particle physics that seeks to understand the nature of elementary particles coming from astronomical origin. This field merges the realms of particle physics, astrophysics, and cosmology all into one exciting frontier of scientific exploration. By studying the interactions of elementary particles with cosmic phenomena, astroparticle physicists aim to unravel the mysteries of the Universe, shedding light on its origins, evolution, and fundamental laws. Astroparticle physics encompasses a wide range of phenomena and concepts, including [1]:

- Cosmic rays: High-energy particles, such as protons and atomic nuclei that originate from sources beyond the solar system and interact with the Earth's atmosphere.
- Neutrinos: Nearly massless particles, which are produced in various astrophysical processes, such as nuclear reactions in the Sun or supernova explosions.
- Dark Matter: A mysterious form of matter that does not emit, absorb, or reflect electromagnetic radiation but exerts gravitational influence on visible matter.

Our journey begins with the introduction of the most fundamental concept in particle physics, the Standard Model.

1.1 The Standard Model of particle physics and nuclear decays

The Standard Model (SM) of particle physics serves as the framework that explains three out of the four fundamental forces known to us in the Universe, namely the electromagnetic, weak, and strong interactions (excluding gravity). Additionally, it categorizes and defines all known elementary particles. As depicted in Fig. 1, in the SM, particles with a spin of 1/2 are divided into two categories: quarks and leptons, each with three generations. The first generation of these particles constitutes ordinary matter, forming stable substances such as protons, neutrons, or atoms. Bosons, which have a spin of 1, are responsible for carrying the forces that affect fermions (particles with half-integer spins). As mentioned, the SM accounts for three fundamental forces: the strong force (transmitted by massless gluons), the

electromagnetic force (transmitted by massless photons), and the weak force, which is mediated by the massive W and Z bosons. Among these, only the W bosons possess electric charge. The Higgs boson lacks both electric charge and color, yet particles interact with it through the Higgs field [2].

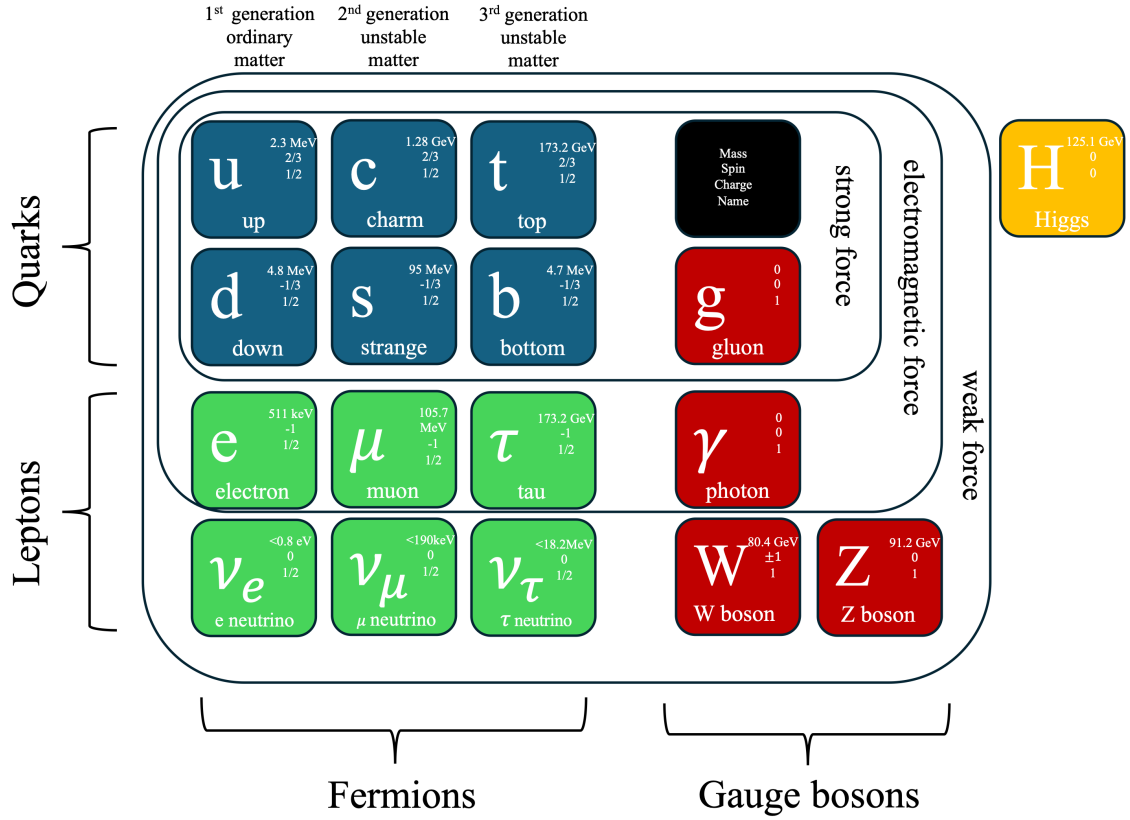

Figure 1: The Standard Model of particle physics. The schematic is based on the information provided in Ref. [3].

However, particle physics is not isolated from other realms of physics. Indeed, it intersects with nuclear physics, particularly in understanding processes like nuclear decays. Let us delve into this intersection to explore how the principles of the Standard Model extend to phenomena such as nuclear decays. There are three leading types of nuclear decays [4]:

- α decay: Parent nucleus emits an alpha particle consisting of two protons (p^+) and two neutrons (n^0)

$$ {}^{A}_{Z}X \rightarrow {}^{A-4}_{Z-2}Y + {}^{4}_{2}\alpha. \tag{1} $$

- β^+ decay: Known as positron emission, occurs when a p^+ within the nucleus is transformed into a n^0, resulting in the emission of a positron (e^+) and an electron neutrino (ν_e)

$$ {}^{A}_{Z}X \rightarrow {}^{A}_{Z-1}Y + e^+ + \nu_e. \tag{2} $$

- β^- decay: Known as electron emission, occurs when a n^0 within the nucleus is transformed into a p^+ , resulting in the emission of an electron and an electron antineutrino ($\bar{\nu}_e$)

$$ {}^{A}_{Z}X \rightarrow {}^{A}_{Z+1}Y + e^- + \bar{\nu}_e. \tag{3} $$

- γ decay: Transition of a nucleus from an excited state to a lower energy state by emission of a high-energy photon, known as the γ particle

$$ {}^{A}_{Z}X^* \rightarrow {}^{A}_{Z}X + \gamma. \tag{4} $$

In particle physics, several conservation laws must be fulfilled for a process to occur. These laws govern fundamental properties such as mass, electric charge, baryon number, and lepton number. According to the SM, each one has to be fulfilled. One important conservation law is the conservation of lepton number, which states that the total lepton number before a reaction must equal the total lepton number after the reaction. Leptons are a type of fundamental particle that includes electrons, muons, taus, and their corresponding neutrinos. Each lepton has a lepton number of +1, while their antiparticles have a lepton number of -1. Other particles, such as quarks and bosons, have a lepton number of 0. The conservation of lepton number is crucial in processes involving weak interactions, such as the aforementioned beta decay, and it ensures that the number of leptons is conserved in these reactions. Even though the conservation of lepton number is a fundamental principle in particle physics, theoretical frameworks suggest the possibility of lepton number violation in certain exotic processes. This would indicate the existence of extensions of the SM. The physical processes that violate the SM are referred to as physics beyond the Standard Model (BSM). In the forthcoming section, an exotic process known as *neutrinoless double-beta decay* is introduced. This phenomenon presents an opportunity to probe potential violations in lepton number conservation.

1.2 Neutrinoless Double-β Decay

In order for the β decay to occur, the binding energy of the daughter nucleus must exceed that of the parent nucleus, as the conversion of a neutron into a proton within the parent nucleus requires an energetically favorable configuration in the resulting daughter nucleus. For some nuclei, such as ^{76}Ge, the isobar one atomic number higher, ^{76}As, has a smaller binding energy, preventing a common β decay [5]. However, the isobar with atomic number two higher, ^{76}Se, has a larger binding energy. Under these conditions, it is possible for the parent nucleus to undergo a *double-beta decay* ($2\nu\beta\beta$), where two neutrons are converted into two protons, accompanied by the emission of two electrons and two antineutrinos as shown in Fig. 2 left. This process was already proposed by Goeppert-Mayer in 1935 [6], and only occurs when the single β decay is highly suppressed. As the ($2\nu\beta\beta$) decay process satisfies all conservation laws, it is consistent with the Standard Model.

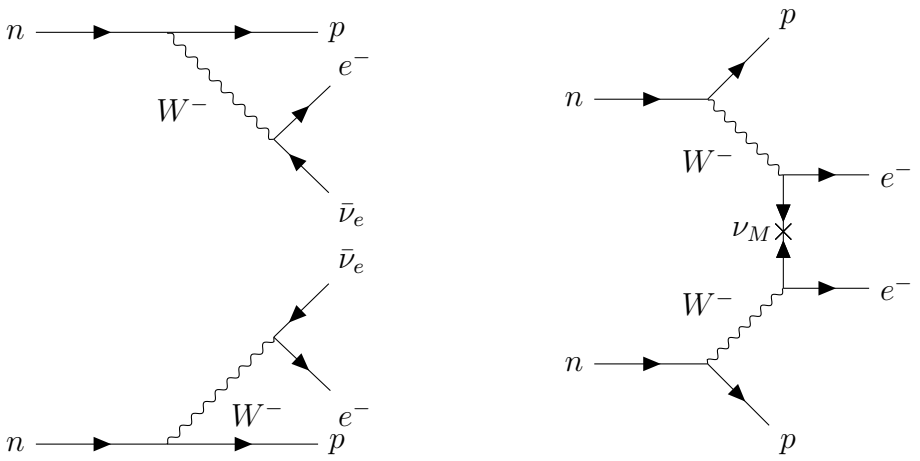

Figure 2: Left: Feynman diagram of $2\nu\beta\beta$ decay compliant with the rules of the SM. Right: Feynman diagram of the $0\nu\beta\beta$ decay, which indicates an extension of the SM, since it violates the conservation of lepton number.

In 1937, the Italian physicist Ettore Majorana revolutionized our understanding of particle physics by hypothesizing the existence of particles that are their own antiparticles [7], a unique property that defies the conventional distinction between matter and antimatter. Particles of this nature were named Majorana fermions, a term often used in opposition to a Dirac fermion, which describes fermions that are distinct from their antiparticle. If the neutrino is indeed a Majorana particle by nature, a second possibility would open for this decay to occur, namely without the emission of antineutrinos. The two antineutrinos would annihilate themselves dur-

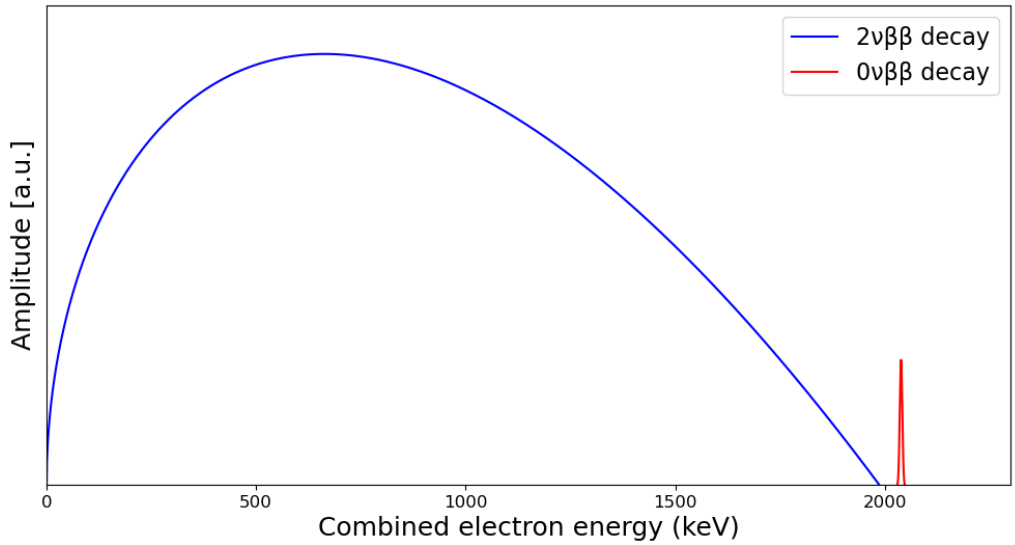

Figure 3: Schematic view of the expected $0\nu\beta\beta$ and $2\nu\beta\beta$ decay amplitude as a function of the combined energies of the emitted electrons. Note that $0\nu\beta\beta$ decay amplitude is unknown.

ing the process, leaving the two electrons as the only emitted particles in the decay, as illustrated in Fig. 2 right, and violating the conservation of lepton number by two units. The observation of the $0\nu\beta\beta$ decay would confirm the possible Majorana-nature of neutrinos [8]. In addition, the observation of lepton number violation, via leptogenesis [9], would give information about the origin of baryon number violation, which is one of three necessary conditions proposed by A. Sakharov in 1967 [10], to possibly explain the production of matter and antimatter at different rates. The $0\nu\beta\beta$ decay is an extremely rare process. The GERmanium Detector Array (GERDA) experiment states in Ref. [11] that the most recent limits on the half-life $T_{1/2}$ of neutrinoless double-beta decay are on the order of 10^{26} years, depending on the isotope. Its signature is a monoenergetic peak at the Q-value of the reaction, which corresponds to the summed energies of the two emitted electrons, whereas in the case of the $2\nu\beta\beta$ decay it is a continuum ranging from zero up to the Q-value, as shown in Fig. 3. To separate a potential signal from various backgrounds, such as neutrino-accompanied double-β decays allowed by the Standard Model, both the energy reconstruction and resolution of the employed detectors are crucial.

2 The LEGEND Experiment

The Large Enriched Germanium Experiment for Neutrinoless double-beta Decay (LEGEND) collaboration was formed as a merger of the two collaborations carrying out leading based $0\nu\beta\beta$ decay experiments, namely the MAJORANA DEMONSTRATOR (MJD) and GERDA, plus additional international institutions. In the first phase of the experimental program, LEGEND-200, up to 200 kg of HPGe detectors will be operated in the cryogenic infrastructure previously installed by the GERDA collaboration at the Laboratori Nazionali del Gran Sasso (LNGS). The targeted sensitivity for discovering $0\nu\beta\beta$ in ^{76}Ge is to reach a half-life of $T^{0\nu}_{1/2} > 10^{27}$ years after five years of data collection. In the second phase of LEGEND, LEGEND-1000, the experiment plans to operate up to 1000 kg of HPGe detectors for a time period of about 10 years. The detectors will be deployed in several payloads. A completely new infrastructure is being built and a more ambitious signal discovery sensitivity on the order of 10^{28} years is targeted [12]. To reach this goal, LEGEND aims to combine the best strategies of both predecessor experiments. The cornerstones are the direct deployment of High Purity Germanium (HPGe) detectors in an active liquid Argon (LAr) shield, as done in GERDA, and the use of ultra-low-activity detector near parts and low-noise front-end electronics, as deployed in MJD [13, 14]. As the successor of the experiments achieving the best energy resolution of 2.52 keV FWHM at the $Q_{\beta\beta}$ (MJD) [15], and the lowest background rates in the field of 5.2×10^{-4} counts/(keV kg yr) (GERDA) [11], LEGEND has the combined expertise required to achieve the $T_{1/2}$ sensitivities needed to search for the $0\nu\beta\beta$ decay signal.

In this section, the technical details of the LEGEND-200 experiment, a cutting-edge endeavor at the forefront of the $0\nu\beta\beta$ decay research, will be discussed. This experiment employs a sophisticated experimental setup, featuring HPGe detectors as its foundation. The crucial role of these detectors in the quest for $0\nu\beta\beta$ decay is addressed, highlighting their exceptional resolution. Additionally, the calibration procedures employed in LEGEND-200 experiment are illustrated, underscoring the significance of precise calibration of the HPGe detectors in achieving reliable and accurate results.

2.1 Experimental setup of LEGEND-200

The LEGEND-200 experiment is located at the *Laboratori Nazionali del Gran Sasso* (LNGS), in L'Aquila, Italy. The experimental halls at LNGS are located under the

Gran Sasso mountain, covered by about 1400 m of rock to protect the experiments from cosmic rays, which is equivalent to 3500 meters of water. Overburden reduces the cosmic muon flux by six orders of magnitude compared to surface levels [16], making it ideal for $0\nu\beta\beta$ decay search, since an ultra-low background is required. Currently, LEGEND-200 operates 101 HPGe detectors summing up to approximately 142.4 kg of mass distributed over ten strings, whereas more detectors will be installed in summer 2024 to reach its planned total mass of 200 kg of ^{76}Ge. The array contains around 70 kg of detectors taken over from MJD and GERDA, with the remainder being new inverted coaxial point contact (ICPC) detectors [17]. Details about the different detector types are described later in this chapter. The detector strings are placed inside a cryostat filled with 64 m^3 of liquid argon (LAr), which cools the detectors to around 87 K, shields them from external backgrounds, and acts as an active scintillation medium. To detect scintillation light, the volume is instrumented with wavelength-shifting fibers surrounding the detector strings (in green in Fig. 4, left), silicon photomultipliers installed on the top and the bottom ends of the fibers, and wavelength-shifting reflectors hung around the detector array (white surface in Fig. 4, right). These can be used to veto background events that deposit their energy in the LAr [18]. The cryostat is immersed in a water tank with a volume of 590 m^3, as shown in Fig. 4, equipped with 64 photomultiplier tubes (PMTs) installed inside the water tank, which serves as a Cherenkov muon detector [19, 20] to further identify background radiation.

LEGEND-200 relies on HPGe detectors, pivotal due to their advantageous properties, particularly well-suited for $0\nu\beta\beta$ decay searches. As briefly mentioned in section 1.2, the search for $0\nu\beta\beta$ decay is based on the detection of a signal peak over the background on the energy spectrum of the summed energies of the emitted electrons. Since the only decay products are the two electrons, their energy is equal to the Q-value of the interaction, which is $Q_{\beta\beta} = 2039.061(7)$ keV [21] for ^{76}Ge. HPGe detectors have the best energy resolution with respect to any other competitive technique with a relative full width at half maximum (FWHM) better than 0.1% at the Q-value of the $0\nu\beta\beta$ decay of ^{76}Ge. This feature allows to identify the γ peaks of the various background sources as well as to isolate the tail of the $2\nu\beta\beta$ decay spectrum from the $0\nu\beta\beta$ decay signal. Since natural germanium has a relatively low natural isotopic abundance of 7.8% for ^{76}Ge, it has to undergo an enrichment process first. Isotopic enrichment is performed in large centrifuge facility. The germanium is converted to the stable gas GeF4 and introduced into a long series of

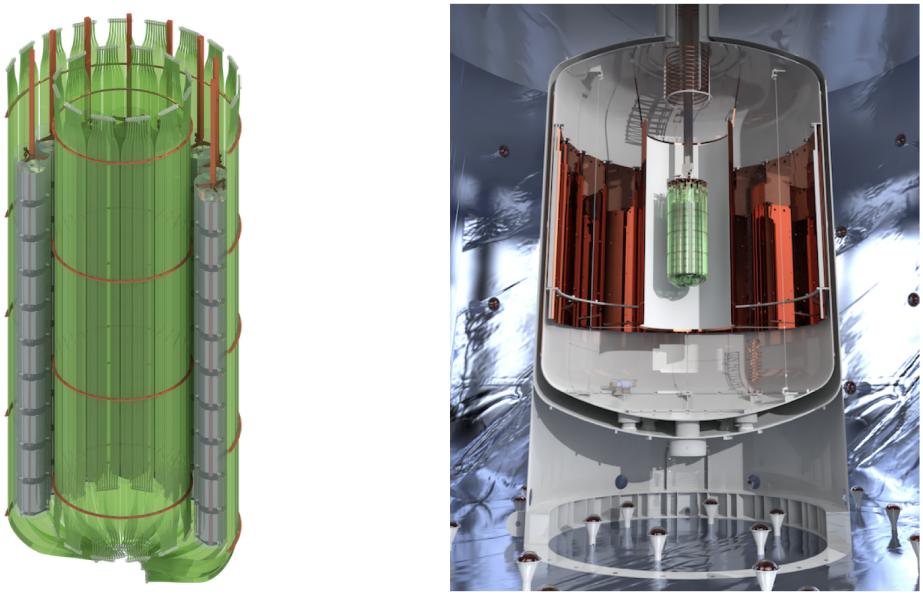

Figure 4: Left: LEGEND-200 Ge detectors mounted in strings and surrounded by optical fibers (in green) that are used to detect the LAr scintillation light. Right: Detector systems positioned in the center of a LAr veto system equipped with wavelength-shifting reflectors. The cryostat is placed in the water tank. Figure taken from [19].

centrifuges. When the required isotopic enrichment is achieved ($> 87\%$), the gas is bubbled into cold water and hydrolyzed [22]. Additionally, the HPGe-based experiments feature a high detection efficiency since the detector is also the source of the $\beta\beta$-decay. HPGe detectors also guarantee a low background level since they have an extremely high intrinsic radio-purity (no measurable U or Th contamination) [23]. Furthermore, delicate analysis techniques such as pulse shape discrimination (PSD) [19, 24] are applied to distinguish signals from background events. Another advantage of the use of the isotope ^{76}Ge is its long half-life of $T_{1/2}^{^{76}\mathrm{Ge}} = (2.022 \pm 0.018_{\mathrm{stat}} \pm 0.038_{\mathrm{sys}}) \times 10^{21}$ years [25], allowing long-duration experiments and the accumulation of large datasets, increasing the statistical power of experiments searching for rare processes like $0\nu\beta\beta$ decay.

HPGe detectors are semiconductor diodes biased at a reverse voltage. Their detection principle is based on collecting charges induced by radiation [18]. There are four different HPGe detector types used in LEGEND: broad energy germanium (BEGe), coaxial (Coax), p-type point contact (PPC), and inverted-coaxial-point-contact (ICPC) detectors. In the Coax design, a bore-hole is excavated along the

central axis to accommodate the p^+ electrode. With such a configuration, relatively large detector masses can be achieved, on the order of 2–3 kg [8]. One major disadvantage of this detector type in comparison to the others is its limited PSD performance [17]. Details about how the PSD technique works is described in Sec. 2.2. The BEGe design, does not include a bore-hole; therefore, the p^+ contact is a small, dot-shaped surface at the center of one of the two detector sides. The absence of a bore-hole makes this kind of detectors harder to be electrically depleted, requiring lower impurity levels and smaller masses, generally less than 1 kg [24, 26]. The main performance feature of the BEGe detectors is their energy resolution of $\sim$ 3 keV FWHM at $Q_{\beta\beta}$ [11]. An excellent resolution does not only allow precise discrimination of the $2\nu\beta\beta$ continuum from the sought-after signal peak, but also enables optimal identification of background γ events [17]. The PPC detectors come originally from the MJD experiment. PPC detectors feature an excellent energy resolution, low detection thresholds down to the sub-keV range, and enhanced background rejection capabilities due to an optimal PSD performance [27]. The newest type of HPGe detectors are the ICPC detectors. These feature a new geometry with respect to the previously used germanium detectors. As shown in Fig. 5, a small p^+ electrode is placed on the opposite face with respect to the bore hole and the n^+ outer contact covers all the remaining surfaces (cylindrical part and bore hole). Detectors without the well (e.g., BEGes or PPCs) are limited to less than 1 kg of mass while ICPC detectors could be produced with a mass larger than 3 kg [28]. This allows increasing the active mass while reducing the amount of nearby materials contributing to the background, such as cables, electronics, and detector holders. Furthermore, because of the long drift time inside the crystal and the small p^+ electrode, the energy resolution and the pulse shape characteristics are very similar to those of BEGe and PPC detectors [29], making this new type of HPGe detectors suitable for $0\nu\beta\beta$ decay experiments [24].

The geometries of the three best types of HPGe detectors are illustrated in Fig. 5. The plot shows the weighting field (E_ω) within a cross section of each detector geometry [19]. The weighting potential refers to the electric potential distribution inside the detector crystal. This distribution determines how the generated charges by incoming radiation move within the detector.

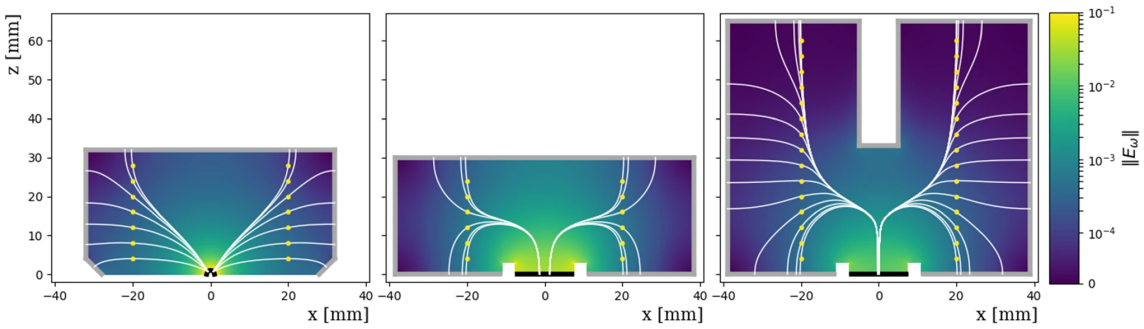

Figure 5: The three detector geometries used in the LEGEND-200 experiment. From left to right: The PPC detector (originally used in MJD), the BEGe detector (originally used in GERDA), and the ICPC detector (originally used in GERDA). Figure from [19].

2.2 Pulse Shape Discrimination

Pulse shape discrimination (PSD) is an analysis method employed in semiconductor detectors, such as germanium crystals, to discern various types of interactions based on the distinctive shapes of the electronic signals they produce. A deep understanding of PSD is crucial in the search for $0\nu\beta\beta$ decay. First, the characteristics of different event-types in the context of the $0\nu\beta\beta$ decay need to be clarified. Events can be classified into single-site (SSE) or multi-site events (MSE). On the one hand, an SSE, as observed in the case of the $0\nu\beta\beta$ decay, is characterized by a single-site energy deposition in the detector bulk of around 1 mm^3 volume [17]. On the other hand, in the case of an MSE, the energy is deposited in multiple parts of the detector, as in the case of many background processes involving high-energy γ interactions. Single-site and multi-site events lead to different shapes of waveforms of the produced charge and current signals. An SSE is characterized by a single current signal, whose amplitude enters a so-called signal acceptance window [17], as shown in the upper left graph in Fig. 6. An equivalent waveform for an SSE is a smoothly rising charge signal, while in the case of an MSE, edges in the charge signal or multiple peaks in the rising current signal are expected. Additionally, this method is also applied to identify events coming from alpha and beta particles depositing energies on the surface of the detectors [20]. Alpha events are characterized by a rapid increase of charge and current signal in a very short time interval, whereas events coming from beta decays are recognizable by a low amplitude in the current signal. This enables a further background rejection by the analysis of the waveforms. The shapes for a few exemplary events are shown in Fig. 6.

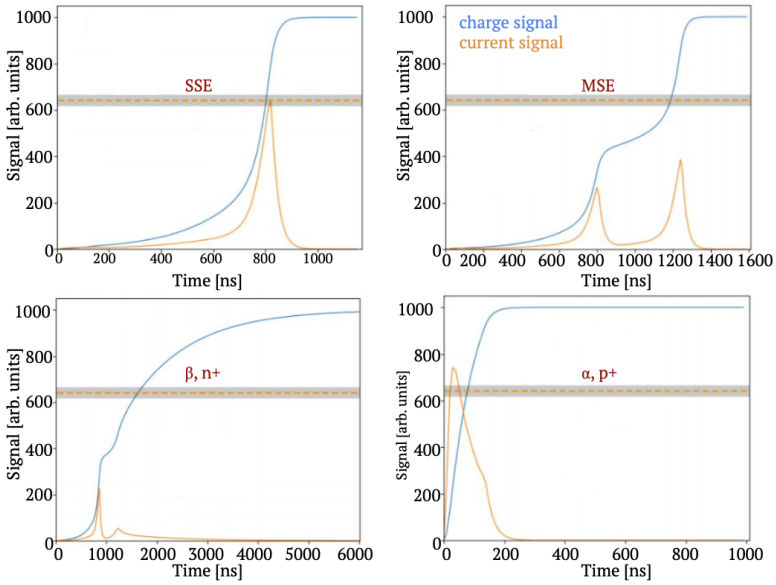

Figure 6: Shapes of waveforms for different event types. The charge signal waveforms are marked in blue and the corresponding current signal waveforms are shown in orange. Top left: Expected waveforms from SSE. Top right: Expected waveforms from MSE. Bottom: Expected waveforms from surface beta (left) and alpha (right) events. Figure from [17].

2.3 Calibration of LEGEND-200

Achieving the necessary precision to detect a signal of $0\nu\beta\beta$ decay requires each HPGe detector's energy scale and resolution to be calibrated with extreme accuracy. To ensure the stability of the energy response and the measured resolution, calibration must be performed frequently. In the LEGEND experiment, radioactive sources are regularly used to irradiate the detector array under controlled conditions. These sources emit γ rays of known energies, allowing precise calibration of the detectors' response within a certain energy range. Additionally, it is crucial to keep any background events induced during calibration below acceptable levels for physics analysis. In this context, the capture of neutrons emitted by the sources is the main concern. Therefore, each source is characterized before being deployed into the experiment [30]. In this section, the strategic selection of the calibration source and the meticulous procedure of the calibration of the LEGEND-200 experiment are addressed.

2.3.1 Energy scale and resolution

The region of interest (ROI) for the $0\nu\beta\beta$ decay search is around $Q_{\beta\beta} = 2039.061(7)$ keV. For the calibration, certain radioactive sources are employed, which emit γ rays as part of their decay processes. These emitted γ rays possess energies ranging from keV to MeV, which cover up the ROI. When these gamma rays interact with the detector, they produce discernible electronic signals, which are typically measured in analog-to-digital-converter (ADC) counts. The energies of these γ rays are well-known and can be accurately determined. This knowledge allows for the establishment of a correspondence between the energy of the detected γ rays and the number of ADC counts recorded. As a result, by histogramming the ADC counts, it becomes feasible to identify energy peaks associated with specific γ ray energies. Following this identification process, a conversion from electronic ADC units to physical energy units (keV/MeV) is conducted. This conversion enables accurate quantification of the energies of the detected γ rays. In Germanium detectors, the energy response is linear to a very good approximation [17]; therefore, it is simple to convert from uncalibrated ADC counts to calibrated energy in keV by applying a linear calibration function. However, due to the different assumptions and approximations in the calibration procedure, slight biases in the energy scale may remain. Such biases may, for example, be caused by the integral non-linearity of the ADCs [31]. Small non-linearities in the energy scale are neglected due to the use of the linear calibration function. Therefore, a peak from a γ ray with a well-defined energy could be displaced towards higher or lower energies. One way of mitigating the bias is to correct for the energy bias of the events that fall into the energy range considered for the $0\nu\beta\beta$ decay search (1930 keV to 2190 keV) by adding the amount of bias to the calibrated event energy [32]. This is possible since the $0\nu\beta\beta$ decay search is extremely sensitive to the energy of the events close to $Q_{\beta\beta}$ and was already done in the final GERDA analysis [11]. Another important aspect of calibration is the energy resolution. As the continuum from the $2\nu\beta\beta$ decay ranges from zero to the $Q_{\beta\beta}$, and the monoenergetic signal from $0\nu\beta\beta$ decay is precisely at $Q_{\beta\beta}$, a limited resolution of the peak could potentially lead to an overlap of both signatures [17]. If the calibration is not precise enough, it is difficult to differentiate between potential events and background. To determine the position and resolution in terms of the full width at half maximum (FWHM $= 2.35 \cdot \sigma$) of the identified energy peaks, fits are performed locally in an energy window of 10–20 keV around the peak position obtained from the calibration. These are configured manually

and separately for each energy peak to avoid interference from neighbouring energy peaks [32]. Finally, all FWHM of the fitted energy peaks are plotted as a function of energy, ranging from 583.19 keV up to 2614.53 keV, as used in the LEGEND-200 standard calibration procedure, and fitted with a best-fit curve, from which the resolution at $Q_{\beta\beta} = 2039.061(7)$ keV can be interpolated for each detector.

2.3.2 Calibration procedure

As the LEGEND-200 experiment reuses the GERDA cryostat with more detector materials and multiple upgraded subsystems, the calibration procedure is very similar to the one used in GERDA. A total of 16 calibration sources evenly distributed on four source insertion systems (SIS) are located around 8 m above the detector array when not in use during physics runs [30]. During calibrations, the sources are lowered by the SIS into the cryostat to the close vicinity of the detectors. They are attached to a stainless steel band whose lower end is connected to a tantalum absorber as shown in Fig. 7. The Ta absorber serves two purposes. First, with a weight of ~ 500 g, it makes sure that the sources are lowered in a vertical path, and the steel band does not fold or rotate, which could lead to a misplacement of the sources in the cryostat. Second, during physics runs, it prevents the γ rays irradiated from the sources from reaching the HPGe detectors. The sources are inserted through a copper funnel into the LAr and positioned next to the detector array. The funnel is needed as the detector array is found to rotate when being deployed into the LAr. The bottom of the absorber is equipped with a polytetrafluoroethylene (PTFE) plate, which enables smooth sliding over the funnels surface to avoid the Ta absorber from getting stuck.

The calibration is performed at the beginning of each week, where calibration data is collected for four to five hours, which corresponds to one calibration run. During the remainder of the week physics data is taken. By irradiating the HPGe detectors with sources of known energy spectra, the detectors' energy responses can be calibrated. It is important to remark that the HPGe detector strings are around one meter long, whereas the sources are distributed over a length of only 320 mm. Thus, to ensure all HPGe detectors get sufficient irradiation, the relative position of the sources is changed after half of the calibration run. The relative positions can be seen in Fig. 12, where the pink squares indicate the position before and blue squares represent the positions after the change of the calibration positions. Currently, only three out of four SIS are operating, because of a technical problem concerning SIS-4.

Therefore, there are no sources depicted in the figure at its position.

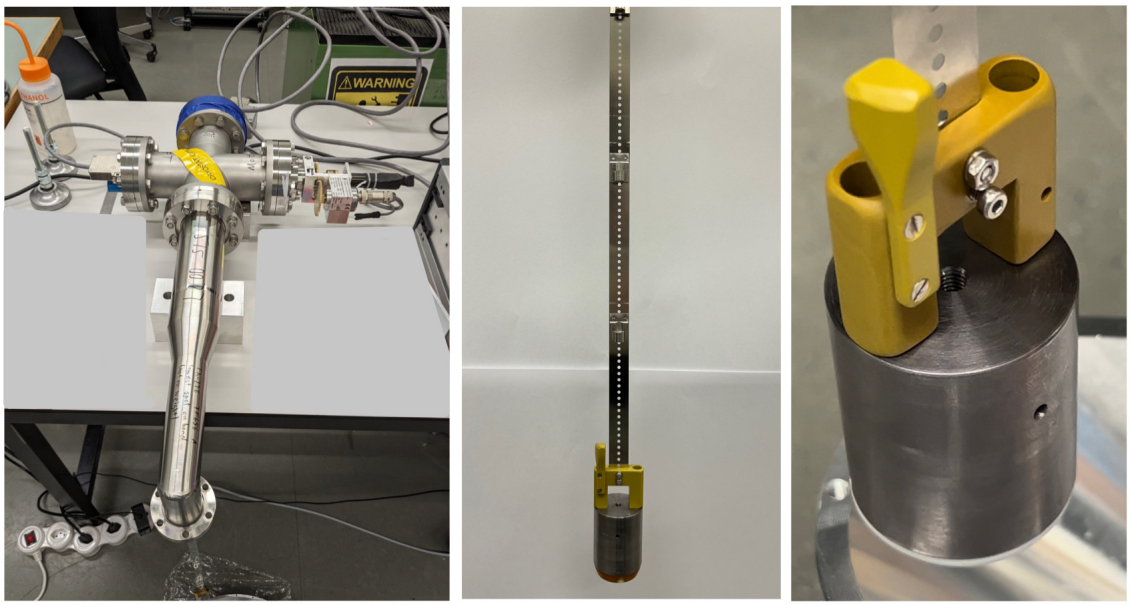

Figure 7: Calibration hardware used in the LEGEND-200 experiment. Left: Source insertion system (SIS) which is mounted on top of the cryostat, from where the calibration sources are lowered. Middle: Stainless steel band with source holders attached. Right: Ta absorber with a PTFE plate fixed at its bottom side to ensure smooth sliding of the absorber over the funnel's surface.

2.3.3 Calibration source

There are many radioactive isotopes that produce γ rays, but not everyone is suitable. For LEGEND-200, as was previously used in GERDA and MJD [32, 33], the isotope ^{228}Th was selected based on the following reasons. Firstly, ^{228}Th undergoes numerous α and β decays before reaching the stable ^{208}Pb isotope. The decay products of the ^{228}Th involve the decay to excited states of several isotopes, subsequently generating monoenergetic γ rays, where a substantial number of high-statistics γ lines lie between 500 and 2614.5 keV, which can be used for calibration up to the $Q_{\beta\beta}$ value. Additionally, the dominant γ line (BR = 33%) at 2614.5 keV, referred to as the full energy peak (FEP), originated from the decay of the isotope ^{208}Tl, is extremely useful for the PSD. This high-energetic γ ray may undergo e^+e^- pair production in the germanium detectors, where the electron deposits energy in the detector while the positron annihilates with an atomic electron in the germanium and creates two annihilation photons [30]. In the HPGe detectors, energy

deposition occurs in one of the three scenarios: both photons deposit energy, only one photon deposits energy, or neither photon deposits energy as shown in Fig. 8. If both photons are detected within the detector, the energy of the FEP is measured. If only one photon is detected and the other escapes from the detector, an energy of 2614.5 - 511.0 = 2103.5 keV is measured. This event is referred to as the single escape peak (SEP). In the case where both photons escape the detectors, an energy of 2614.5 - 2·511.0 = 1592.5 keV is measured. This event is called the double escape peak (DEP). The DEP is topologically equivalent to the signal coming from $0\nu\beta\beta$. As both the DEP coming from the ^{208}Tl decay and the $0\nu\beta\beta$ signal are SSE, they produce similar waveforms; therefore, the DEP is used to calibrate the PSD techniques.

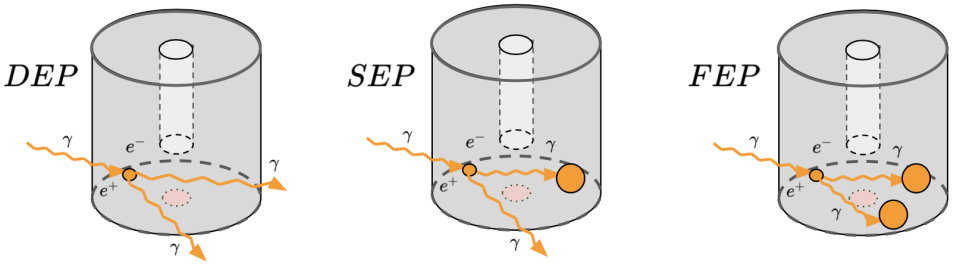

Figure 8: The three scenarios from the interaction of the 2614.5 keV ^{208}Tl line. From left to right: double escape peak (DEP), single escape peak (SEP), full energy peak (FEP). Figure from [17] made by C. Scaffidi.

An additional benefit of utilizing ^{228}Th is its relatively long half-life of approximately $T_{1/2} \approx 1.9$ years. However, the sources still decay away during the typical experimental runtime of around 5 years. Consequently, while source replacements are necessary, they are less frequent compared to isotopes with shorter half-lives. An undesirable feature of ^{228}Th is its neutron emission via (alpha, n) reaction. This emission can lead to the activation of ^{76}Ge, resulting in the production of ^{77}Ge (half-life 11.3 h) and ^{77m}Ge (half-life 53.7 s) isotopes. These isotopes subsequently undergo β decays with Q-values exceeding 2 MeV. Additionally, neutrons can be captured by surrounding materials, producing high-energetic γ rays [30]. Fortunately, the neutron flux can be reduced by embedding the ^{228}Th sources in gold. The neutron background in LEGEND-200, as induced by calibration runs, was estimated to be $\mathcal{O}(10^{-5})$ ($\mathcal{O}(10^{-7})$) events/(keV·kg·yr) before (after) background reduction cuts [19]. Compared to the LEGEND-200 background goal of $\mathcal{O}(10^{-5})$ events/(keV·kg·yr) after cuts, the estimated value is considered sufficiently low to safely deploy the radioac-

tive sources in the experiment [30]. The production method and the characterization of the ^{228}Th sources deployed in LEGEND-200 is detailed in Ref. [30].

3 Data Analysis – Calibration in the low-energy regime

In this section, the results obtained from two calibration runs of different periods are shown. Fig. 9 shows the energy spectrum of an exemplary ICPC detector. The dashed gray lines are seven energy peaks used in general LEGEND-200 analysis ranging from 583 to 2614.5 keV. From 500 keV downwards, no further energy peaks are used for calibration. The main reason is that the ROI of the $0\nu\beta\beta$ decay in ^{76}Ge lies around the Q-value of $Q_{\beta\beta} = 2039.061$ keV [32].

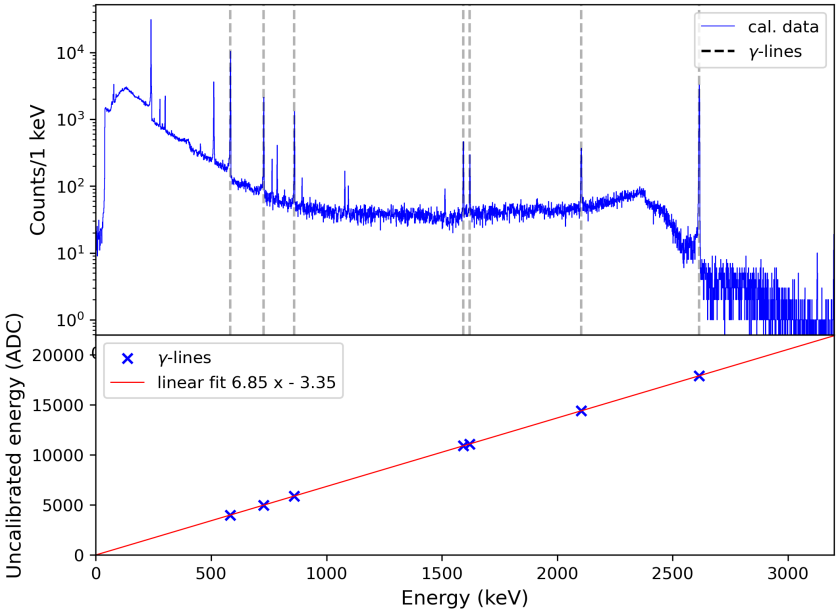

Figure 9: Top: calibrated energy spectrum for the detector channel V02160B. The dashed grey lines indicate the detected peaks. Bottom: linear calibration curve for the corresponding detector as determined by a linear fit of the mean positions of the detected peaks.

Adding low energy peaks might make the HPGe detectors more sensitive to other BSM processes involving lower energies. In this section, the initial focus lies on the exploration of potential coincidental occurrences within proximate detectors. A comparative analysis of energy spectra from paired detectors was undertaken, aiming to search for preferred combinations of the partial energy depositions in each detector in a pair. Subsequently, energy peaks that are not used in the standard LEGEND-200 calibration were found, and we studied the potential of integrating these peaks into the standard calibration procedure.

3.1 Coincident events in nearby detectors to look for possible low-energy events

One of the primary objectives of our study is to explore the phenomenon wherein a photon emitted from a γ decay event may deposit its energy in two nearby detectors. Specifically, the aim is to investigate scenarios where a photon initially interacts with and deposits some energy in one detector (referred to as detector A) before continuing its trajectory and depositing the remaining energy in an adjacent detector (referred to as detector B), as shown in Fig. 11. The goal is to examine, if there is a preferred combination for the measured energy depositions. A preferred partial energy deposition, where the deposited energies stay constant over time, result in an energy peak in the corresponding energy spectrum, which could be used for calibration of the HPGe detectors. As this process involves more than one detector, a method where data from multiple detectors can be examined concurrently, is needed. A two dimensional histogram is a suitable method for carrying out this analysis, as the data from two detectors can be superimposed and thus any traces of simultaneity recognized. This process involves the photon undergoing Compton scattering within detector A, resulting in a partial energy deposition. Subsequently, the photon continues its path, potentially interacting with detector B and depositing the remainder of its energy via photoelectric absorption. This is only possible, if the initial energy of the photon lies in the energy range, where the cross section for Compton scattering of photon processes in ^{76}Ge is dominant over other processes. The absorption coefficients for photon processes as a function of the photon's energy are depicted in Fig. 10.

Understanding and characterizing such energy deposition patterns is important for several reasons. Firstly, it provides information about the behavior of photons in detector materials, as well as their interactions and energy transfer processes. Secondly, this phenomenon has implications for the accurate calibration of detector systems, particularly in scenarios where multiple detectors are arranged nearby, as is the case in the LEGEND experiment. Fig. 12 illustrates the spatial configuration of the 101 HPGe detectors, categorized by their respective types, alongside the distribution of the radioactive ^{228}Th calibration sources across three strings. It is noteworthy that a fourth string, designated for the SIS-4, is presently inactive.

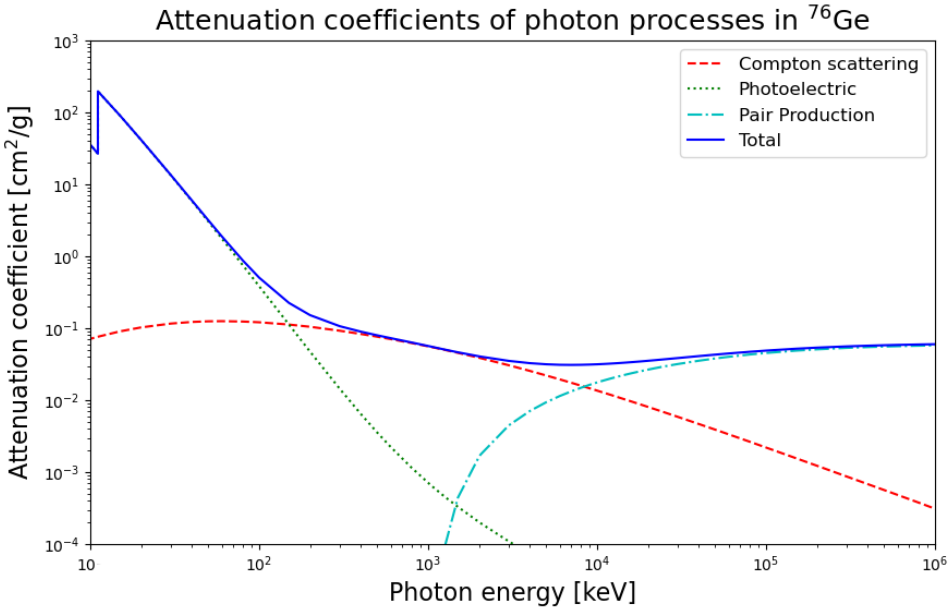

Figure 10: Attenuation coefficients for photon-matter interactions as a function of energy. Data from [34].

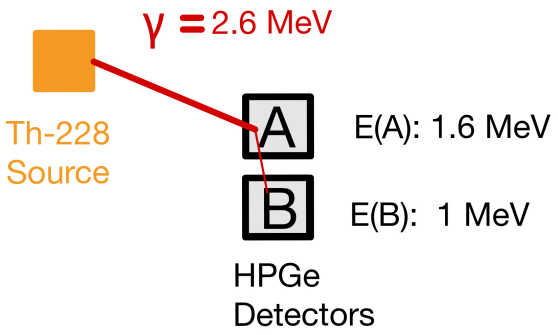

Figure 11: Concept of coincident events in nearby detectors. An exemplary photon of 2.6 MeV undergoes Compton scattering in detector A, while depositing part of its initial energy, e.g., 1.6 MeV. The scattered photon deposits the remaining 1 MeV of its energy in detector B via photoelectric absorption.

3.1.1 Coincident events in two nearby detectors

To increase the probability of observing coincident events, strategic selection of detector pairs is crucial. Preference is given to pairs positioned next to each other, ideally in close proximity to calibration sources. Furthermore, in our investigation into the detector dependence, combinations involving various detector types were explored. To ensure the proper working of our code, firstly the focus lied on the full

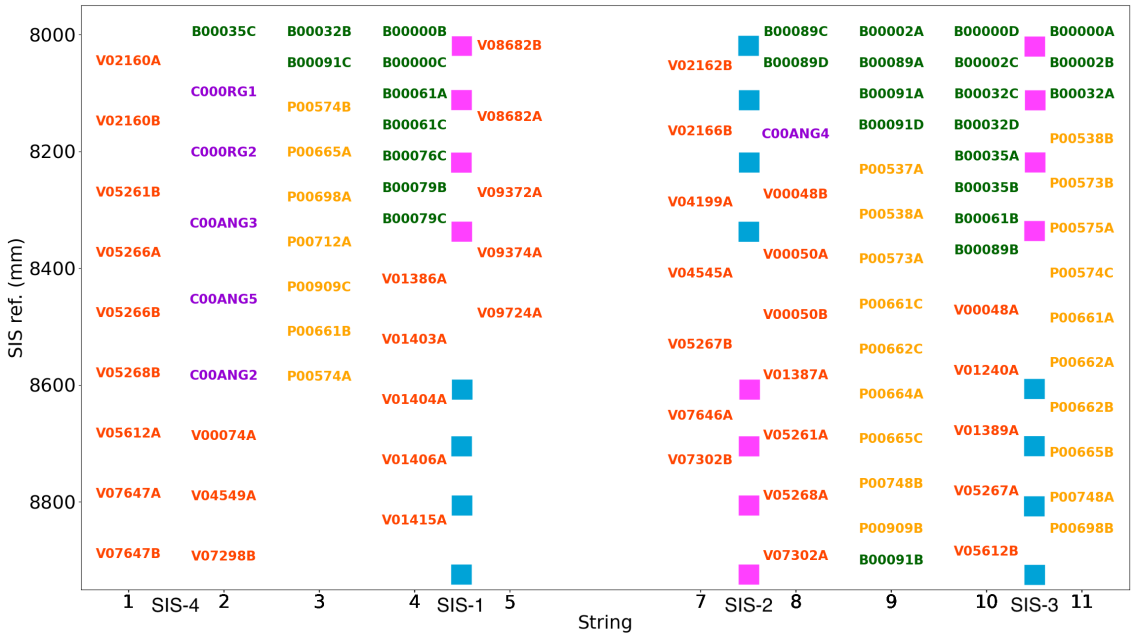

Figure 12: Locations of the HPGe detectors and calibration sources in the LEGEND-200 experiment. Detectors are identified by their detector ID: Detector IDs in orange and starting with 'V' are ICPC detectors. Detector IDs in green and starting with 'B' are of BEGe type. Detector IDs in purple and starting with 'C' are Coax detectors. Detector IDs in xellow and starting with 'P' are PPC detectors.

energy range. As depicted in Fig. 9, the presence of peaks is expected to manifest as distinct vertical and horizontal lines corresponding to their respective energies. Note that the manifestation of a vertical or horizontal line serves as a definitive indication of a single detector absorbing the entirety of the photon energy. From Fig. 13 the signatures of the expected distinct energy peaks from the decay chain of ^{228}Th can be seen as straight lines. A large area appears saturated at lower energies, characterized by more than 15 counts per bin, reflecting the imposed limit on the plot.

In this study the focus lies on the energy range of 50 keV to 238 keV. This selection is deliberate, as in the LEGEND-200 experiment, the detectors are calibrated down to 583 keV, which is the lowest energy peak used for the usual calibration. The potential of calibrating down to 238 keV has been studied; however, beyond this point downwards, lies unexplored territory concerning the calibration of the HPGe detectors in LEGEND-200. The lower bound of 50 keV for the energy range is established as it serves as a threshold to mitigate background noise originating from electronic sources. As was already introduced in Sec. 3.1, the initial energy of the

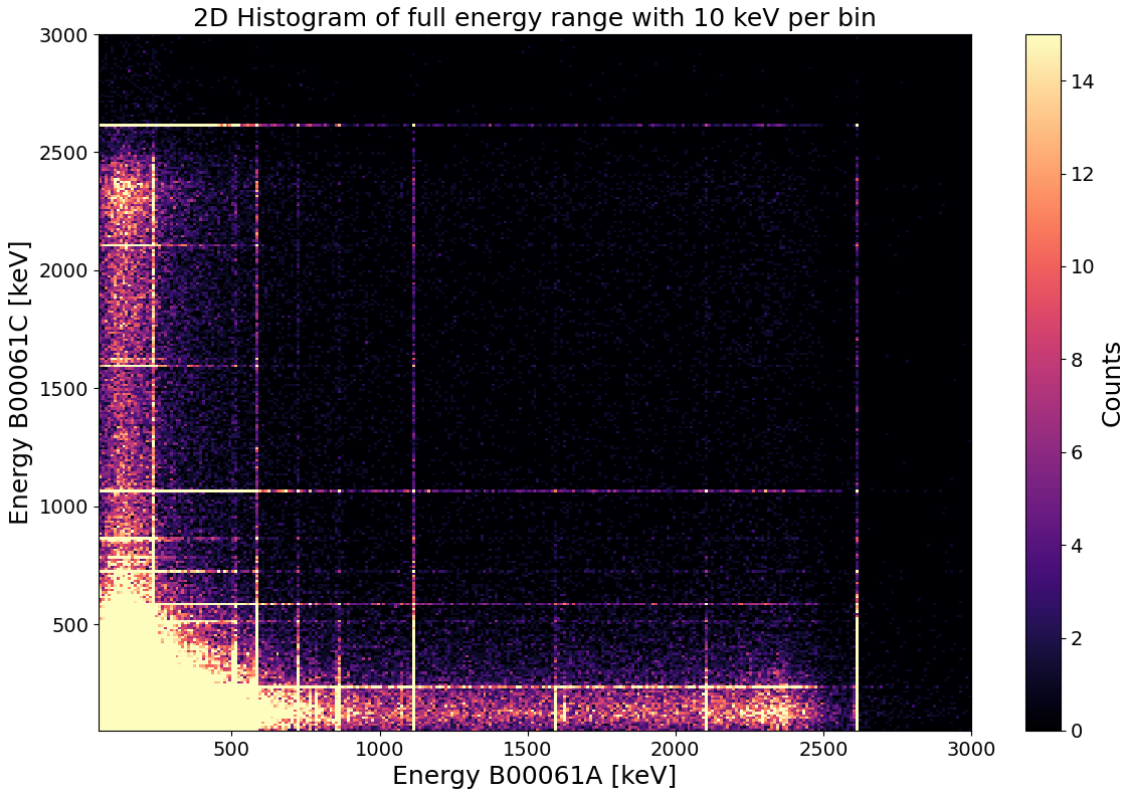

Figure 13: 2D histogram of energy depositions in two nearby detectors B00061A and B00061C. The energy peaks coming γ rays of the ^{228}Th sources are visible for both detectors shown as vertical and horizontal lines.

photon must lie in the energy range, where the cross section for Compton scattering is dominant over other processes. For photons inside the energy range of 50 keV to 238 keV this is not the case, since the cross section for photoelectric absorption is higher by up to two orders of magnitude as can be seen from Fig. 10. Therefore the probability of observing coincident events in this energy range is low. As previously mentioned, the presence of a horizontal or a vertical line serves as an indicator of complete photon energy absorption by a single detector, a key signature to identify. Another notable signature is the appearance of a hotspot in a 2D histogram. A hotspot suggests partial energy deposition across multiple detectors, where the combined X and Y coordinates of the histogram should align with the total energy of the scattered photon. This study was conducted for ten detector combinations, which were selected based on their positions with respect to the source and their detector types. Detector combinations of pure ICPC and BEGe as well as mixing of ICPC with BEGe, ICPC with Coaxial, and BEGe with Coaxial detectors were

selected to investigate on the possible detector type dependence. The results of this study are summarized in Fig. 14 with more histograms shown in appendix A. As some detectors recorded more counts than the others, the scale for each detector combination had to be adjusted individually, such that the data became visible. All histograms exhibit a large blot of counts, ranging from approximately 80 to 200 keV, which can be seen from the calibrated energy spectrum as shown in Fig. 9 manifesting a high level of counts in lower energies. Clear hotspots that would indicate a preferred combination in the partial energy depositions in two detectors were not observed.

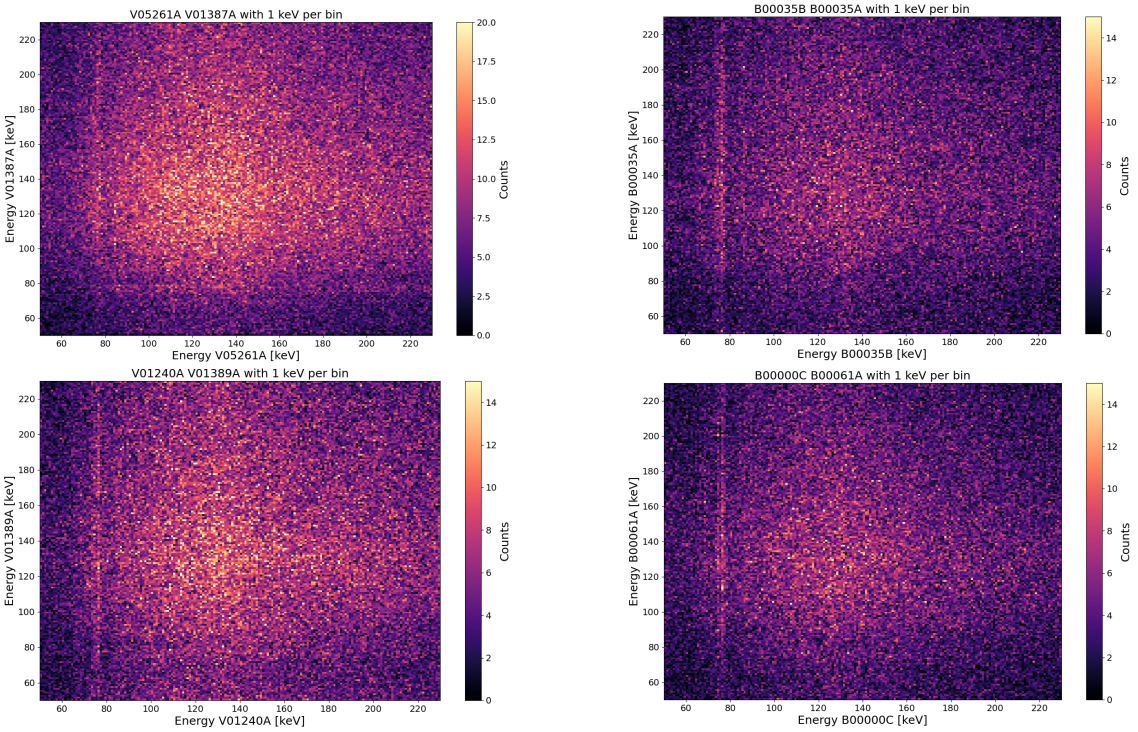

Figure 14: Top left: ICPC detector combination: V01387A vs V05261A. Top right: BEGe detector combination: B00035A vs B00035B. Bottom left: ICPC detector combination: V01240A vs V01389A. Bottom right: BEGe detector combination: B00000C vs B00061A.

At around 74-77 keV, a line is visible; hence, further analysis was carried out to examine this energy region. To refine the estimation of the energy associated with the observed gamma peak, Fig. 15 shows a histogram with smaller bin sizes (0.5 keV instead of 1 keV). This allows a more detailed visualization of the peak. Additionally, a one-dimensional energy spectrum was constructed specifically for the detectors that captured the peak, focusing on the energy range between 50 and

100 keV to enhance clarity and precision. Upon employing smaller bin sizes, it was observed that the energy line originally sought after is a combination of two energy peaks, as can be seen from the one-dimensional energy spectrum shown in Fig. 15. To confirm this hypothesis, attention is turned to the one-dimensional energy spectrum of detector B00000C. Here, the conjecture finds support as two distinct peaks within the 74-77 keV range are observed. Furthermore, the literature values from the gamma energies in the ^{228}Th decay chain in the energy range of 74-77 keV were investigated, to see if there is an actual physical process behind the observation, or if it was just background signals from the electronics. The possible candidates are summarized in table 1.

Isotope	Energy [keV]	Intensity [%]
^{228}Th	74.400	3.9×10^{-4}
^{216}Po	74.969	7.0×10^{-6}
^{212}Pb	74.815	9.9 %
^{212}Pb	77.107	16.4 %
^{208}Tl	74.969	3.35 %

Table 1: Physical gamma energies in the ^{228}Th decay chain in the energy range 74-77 keV with their respective intensity [35, 36].

The gamma peaks from ^{228}Th and ^{216}Po show intensities of at least four orders of magnitude less than the other candidates. The peak from ^{212}Pb at 74.815 keV is close to the one from ^{208}Tl at 74.969 keV and has a larger intensity by a factor of three. So from now on, only the two candidates with the largest intensity will be considered:

- ^{212}Pb at 74.815 keV,
- ^{212}Pb at 77.107 keV.

In Fig. 15, the two energies of the candidates are marked with dashed lines in the one-dimensional energy spectrum. The observed energy peaks in the spectrum align well with the inserted lines. It is worth noting that a linear polynomial fit was employed to convert the analog ADC counts to the unit of energy. This is an indicator for the high accuracy of the linear conversion between uncalibrated and calibrated energy.

Having found energy peaks at 74.815 keV and 77.107 keV opens up the opportunity to use them in the usual calibration procedure. As mentioned in Sec. 2.3, the

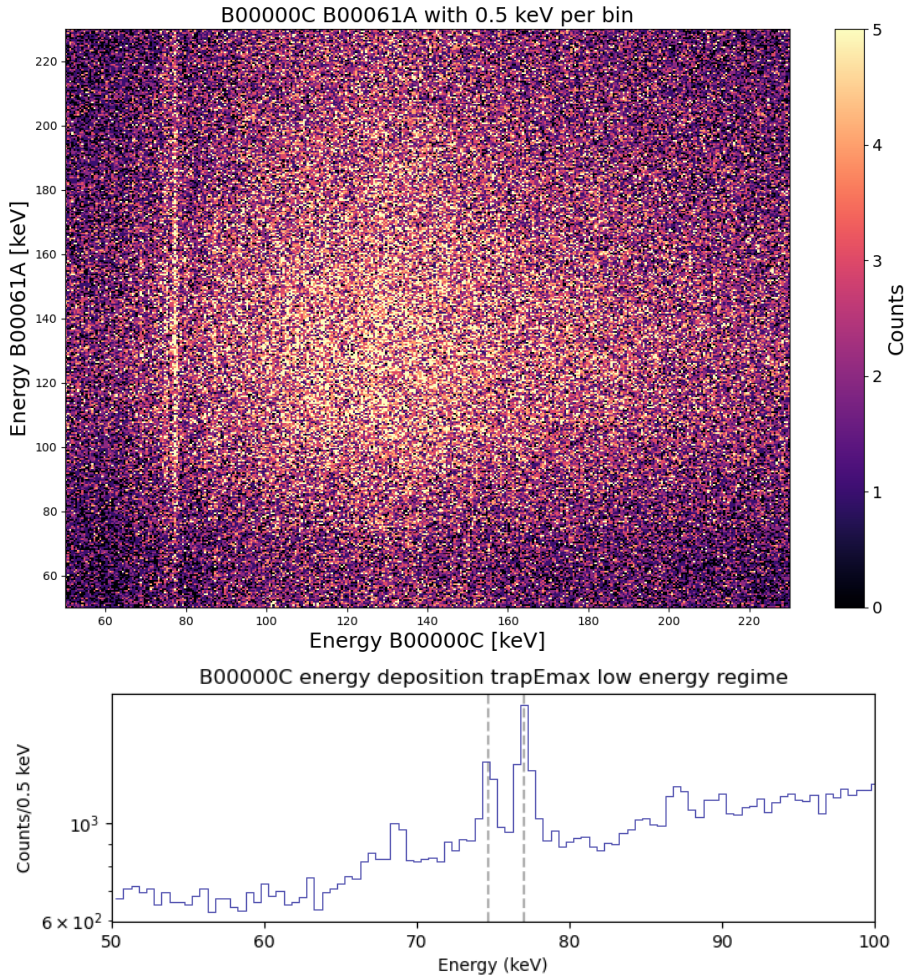

Figure 15: Top: 2D histogram of detectors B00061A and B00000C with a bin size of 0.5 keV. Bottom: 1D energy spectrum of detector B00000C in the range of 50-100 keV.

HPGe detectors are calibrated by matching the observed peaks in the uncalibrated energy spectrum to known energy peaks. The study to investigate the potential of integrating these two energy peaks into the standard calibration procedure is detailed in Sec. 3.2.

3.1.2 Energy correlation for two detectors

In many different gamma-ray detection systems, the events are registered in coincidence, i.e., within short time intervals, by two or more detectors, when coming from the same initial photon. In calibration, this phenomenon is useful for many reasons. On the one hand, if the photon interacting with multiple detectors leads

to a preferred combination of the partial energy depositions, this would manifest as a peak in the 1D energy spectrum, which can be used to calibrate the detector, as already motivated in Sec. 3.1. On the other hand, observing events of partial energy depositions can also be favorable for PSD. As a photon undergoes Compton scattering in the first and then is absorbed via photoelectric effect in a second detector, the scattered photon would most likely deposit its energy in a very localized part of the germanium materials in the second detector, categorized an SSE. The produced waveforms of these events can be used to train PSD algorithms. In order to investigate coincident events of a corresponding γ, the energies of the deposited events of nearby detectors were displayed in a 2D histogram, and we searched for an anti-diagonal line between a given energy peak in both detectors. This anti-diagonal line is evidence for coincident events in both detectors coming from the same initial photon with the given energy. This means that the sum of X and Y coordinates of the events within the line is constant and equal to the initial energy of the photon. An essential consideration in this study revolves around the temporal dimension. Given our focus on identifying coincidental events, it is important to restrict our analysis to a very brief time interval. As the time interval extends, the correlation between events diminishes, making it increasingly challenging to discern the anti-diagonal correlation line [37]. Therefore, in order to avoid this, a Δt matrix was constructed, where the entries represent the absolute value of difference in timestamps of all recorded events in two nearby detectors. An illustration of Δt matrix is shown in Eq. 5. The minimum entry value of the matrix was computed, and a threshold value slightly higher than that minimum was chosen to increase the probability of including coincident events.

$$\begin{bmatrix} |t(\text{event 1 detector A}) - t(\text{event 1 detector B})| & \cdots & |t(\text{event 1 detector A}) - t(\text{event n detector B})| \\ \vdots & \ddots & \vdots \\ |t(\text{event m detector A}) - t(\text{event 1 detector B})| & \cdots & |t(\text{event m detector A}) - t(\text{event n detector B})| \end{bmatrix} \tag{5}$$

For this study, the focus lied on two combinations of neighboring detectors where the newly discovered low-energy peak has been observed: B00061C/B00076C and B00035B/B00061B. As depicted in Fig. 16, the anti-diagonal correlation line is observable for both detector combinations when analyzing the two peaks at 2614.5 and 583 keV. As mentioned in Sec. 3.1.1, the energy threshold of individual detectors is 50 keV, making it in principle impossible to observe coincident events coming from a photon with an energy of less than 100 keV, since any combination of energies adding up to less than 100 has at least one component below the energy threshold

of 50 keV and is not recorded.

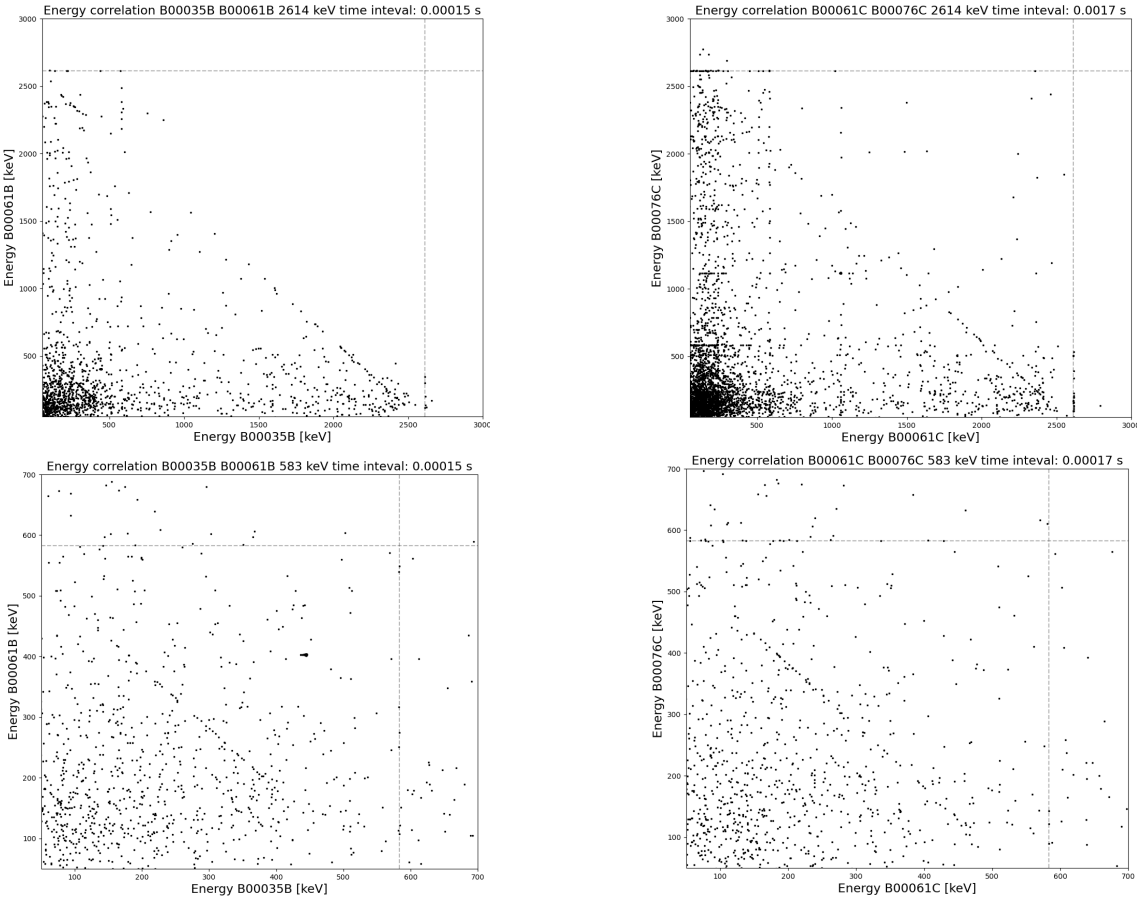

Figure 16: Energy correlation of two detectors in calibration period 07, run 002. Due to the small amount of statistics, the color bar of the 2D hist has been removed. The plots are no longer 2D histograms, but scatter plots of events. Every event represents one single count. Top: Energy correlation of the 2614.5 keV peak. Bottom: Energy correlation for the 583 keV peak.

As previously stated, the anti-diagonal correlation line for the 77 keV peak cannot be observed because of the electronic threshold at 50 keV for HPGe detectors. If there were supposedly no data cuts below 50 keV, it would still be improbable to observe coincident events for such low energy events. The reason is provided by the cross sections of photon-matter interactions in germanium in Fig. 10. We recall that to observe coincident events the photon must undergo Compton scattering in the first and photoelectric absorption in the second detector. For an energy of 77 keV the dominant process is the photoelectric effect, as its cross section is higher by one order of magnitude with respect to the Compton effect, making the observation of

coincident events unlikely. Furthermore, due to the relatively small signal-to-noise ratio (SNR) in the low-energy regime, energy correlation would become even more difficult to observe. Higher SNR enhances correlation visibility, as illustrated in Fig. 9, where the SNR for the FEP and 583 keV peak is notably higher compared to lower energies. Another potential limitation can be the presence of the LAr shield surrounding the HPGe detectors in LEGEND-200, functioning as a veto system for background processes. It is conceivable that photons with low energies deposit part of their energy in one detector but lack sufficient energy to penetrate the LAr shield and deposit the remaining energy in the second detector. These factors suggest that the chance to observe coincident events in nearby detectors originated from photons at 74-77 keV is close to zero.

As mentioned above, if a photon undergoes Compton scattering in a first detector and photoelectric absorption in a second detector, this could be useful for pulse-shape analysis, since the energy deposition in the second detector is an SSE and thus has a topological analog waveform as the signal from a candidate of $0\nu\beta\beta$ decay. Depicted in Fig. 16 are events close to the edges of the correlation lines, as one of the two energy depositions has lower energies, they have a high probability to undergo photoelectric absorption. Hence, this type of events can be used for machine learning algorithms to train the PSD and thus improve the background analysis methods.

3.2 New low-energy peaks for calibration of HPGe detectors

In the preceding section, it was concluded that no preferred combination of the partial energy depositions serve as additional energy peaks for calibration was observed. Furthermore, the 74.815 and 77.107 keV energy peaks are not suitable for the coincidence study because of the 50 keV energy threshold of the experiment. However, the observed 74.815 and 77.107 keV peaks could be included into the calibration procedure, enhancing sensitivity of our detectors to low-energy processes. Furthermore, the potential of improving the resolution at the Q-value of $Q_{\beta\beta} = 2039.061$ keV was investigated. In the usual calibration procedure of LEGEND-200 the peaks at 583.2 keV, 727.3 keV, 860.5 keV, 1592.5 keV (DEP), 1620.50 keV, 2103.5 keV (SEP), and 2614.5 keV (FEP) [32] are selected. To increase the coverage of the calibrated energy range, five additional low energy peaks used in the Majorana Demonstrator [33] and the two peaks at 74.815 and 77.107 keV, are included. The used energy peaks as

well as their respective parent nuclei and intensities are summarized in table 2.

Isotope	Energy [keV]	Intensity [%]
^{212}Pb	74.815	9.9 %
^{212}Pb	77.107	16.4 %
*^{212}Pb	238.63	43.3 %
*^{224}Ra	240.99	4.1 %
*^{208}Tl	277.36	2.3 %
*^{212}Pb	300.09	3.2 %
*^{208}Tl	510.77	20.60 %
**^{208}Tl	583.19	30.4 %
**^{212}Bi	727.33	6.5 %
**^{208}Tl	860.56	4.4 %
**^{208}Tl (DEP)	1592.5	3.35 %
**^{212}Bi	1620.50	1.47 %
**^{208}Tl (SEP)	2103.5	3.35 %
**^{208}Tl (FEP)	2614.53	35.6 %

Table 2: Used energy peaks for the calibration of the HPGe detectors with their respective parent nucleus and intensity.
*additional peaks used in MJD
**peak used in LEGEND-200

All 101 HPGe detectors were calibrated for two different and randomly selected calibration runs, period 07, run 008 and period 08, run 002, using these additional low-energy peaks. The calibration procedure is divided into several steps. First, the raw data (ADC counts) were histogrammed using a function from the pygama library to obtain the uncalibrated energy spectrum of the detector. The pygama library in Python is a package specifically designed for data processing and analysis related to cryogenic germanium detectors. Then, a peak search was conducted, where a peak was defined as a five sigma deviation from the neighboring bins. Next, the electronic signals were calibrated to physical energy units (keV) using a polynomial fit to the known energy peaks. In this step, a polynomial fit of first and second degree was performed to investigate, if the linear energy response of HPGe detectors was still valid in lower energies. Furthermore, fit functions modified from the pygama library were employed to fit the peaks, followed by the generation of the resolution curve, used to interpolate the energy resolution at $Q_{\beta\beta}$, a critical step of the calibration procedure. After running the calibration code for all 101 HPGe detectors for both calibration runs, the following results were obtained:

- period 07, run 008: 12/101 HPGe detectors detected 77.107 keV as a peak
  5/12 HPGe detectors detected 74.815 keV as a peak
- period 08, run 002: 10/101 HPGe detectors detected 77.107 keV as a peak
  2/10 HPGe detectors detected 74.815 keV as a peak

The 74.815 keV peak has only been observed in conjunction with the 77.107 keV peak, with no instances of solitary detection recorded. The detailed list of the detectors that identified the 77 .107 keV peaks can be found in the appendix B. Upon comparing their locations relative to the source positions shown in Fig. 12, it was observed that only detectors situated in close proximity to the calibration sources successfully detected the peaks mentioned above. Detectors positioned within strings 1, 2, 3, or 9, strings that are not directly adjacent to the calibration sources, failed to register these peaks. Notably, string 6, which is currently empty, is omitted from this discussion. In both selected calibration runs, the detector B00000C, which is positioned in string 4 second from the top and is of a BEGe type, identified both low energy peaks. Besides, a source is in close proximity, which is crucial for the identification of the low-energy peaks. In Fig. 17, the uncalibrated and the calibrated energy spectra are shown, as well as the calibration curve and the residuals, both with linear and quadratic approximations. Note that in the figure of the calibration curve only the red curve (quadratic fit) is observable, since both calibration curves overlap exactly. The residuals vary from +0.5 keV to -0.5 keV. It is difficult to decide if the linear or the quadratic approximation is more suitable based on these results. One could conduct a study, where the residuals of both approximations are histogrammed together. The mean values could be extrapolated and one should be able to decide, which one is more suitable by comparing their deviation from zero.

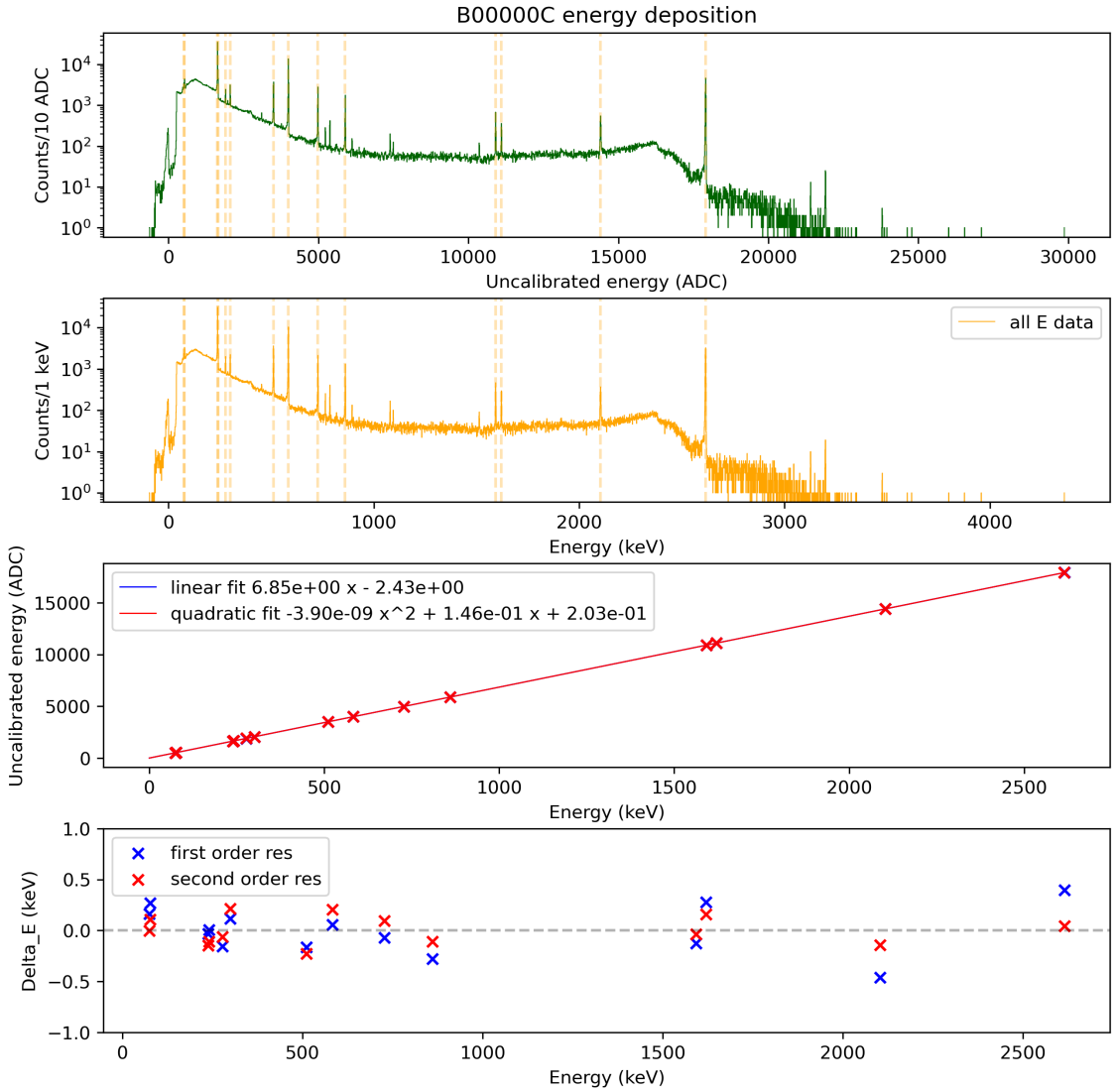

Figure 17: From top to bottom: Uncalibrated energy spectrum, calibrated energy spectrum, linear/quadratic calibration curve, linear/quadratic residual plot for detector B00000C. The dashed lines in the top two plots indicate the position of the identified peaks in the respective energy spectra.

4 Results

In this chapter, the results of the resolutions of the HPGe detectors are presented. As mentioned in Sec. 2.3.1, to find the resolution at $Q_{\beta\beta}$, the used peaks need to be fitted and the FWHM calculated. The FWHM of all peaks is then plotted as a function of energy and by using a best fit curve, the resolution (FWHM), at $Q_{\beta\beta}$ is interpolated. Furthermore, the obtained resolutions for the detectors will be compared to the resolution values from the official LEGEND-200 data. The corresponding calibration steps for an exemplary detector B0000C are shown here, whereas the results for the other HPGe detectors are similar.

After identifying the peaks from the energy spectrum, all energy peaks were fitted with predefined fit functions from the pygama library. These fit functions incorporate key components to accurately model the observed data. They comprise a Gaussian peak, representing the primary energy emission, characterized by parameters including the peak position and the width. Additionally, a low-energy tail factorizes tailing effects, while a noise pedestal accounts for background signals and electronic noise. Overall, these components collectively enable precise extraction of peak parameters and background estimation in γ-ray spectra. In particular, the fitting of the peaks at 74.815/77.107 keV and 238.62/240.99 keV respectively caused difficulties, as in both cases there are two energy peaks that are close to each other, making the distinctiveness challenging. In this case, a special double-peak fit function was employed. On the one hand, the double peak at 238/240 keV was fitted properly. For the previously found low-energy peaks, on the other hand, slight manual adjustments had to be made on the individual fit parameters and the fitting had to be performed multiple times until an acceptable result was accomplished. Nevertheless, a precise fitting of the tails remained a challenge. A possible reason for the difficult fitting is the low SNR of the peaks at 74-77 keV, which can cause challenges for recognition of the peaks. This resulted in a relatively small p-value compared to other fitted peaks. Remember, a p-value less than 0.05 is typically considered to be statistically insignificant, in which case the null hypothesis, i.e., our fitted curve, should be rejected meaning that the fit is not precise enough. An example of the fitted peaks is depicted in Fig. 18. The double peaks of 74.815/77.107 keV were fitted well at the peak positions albeit the low p-value, which is most likely because of the misfitted tails. An alternative useful approach for this specific case would have been to utilize the branching ratio. Since both 77.107 keV and 74.815

keV are emitted from the ^{212}Pb, the relative branching ratio (given in table 2 as the intensity) can be used to eliminate a fit parameter by expressing the amplitude of the 74.815 keV peak as a function of the amplitude of the 77.107 keV peak. By reducing the number of fit parameters the fits might potentially improve as they are more constrained.

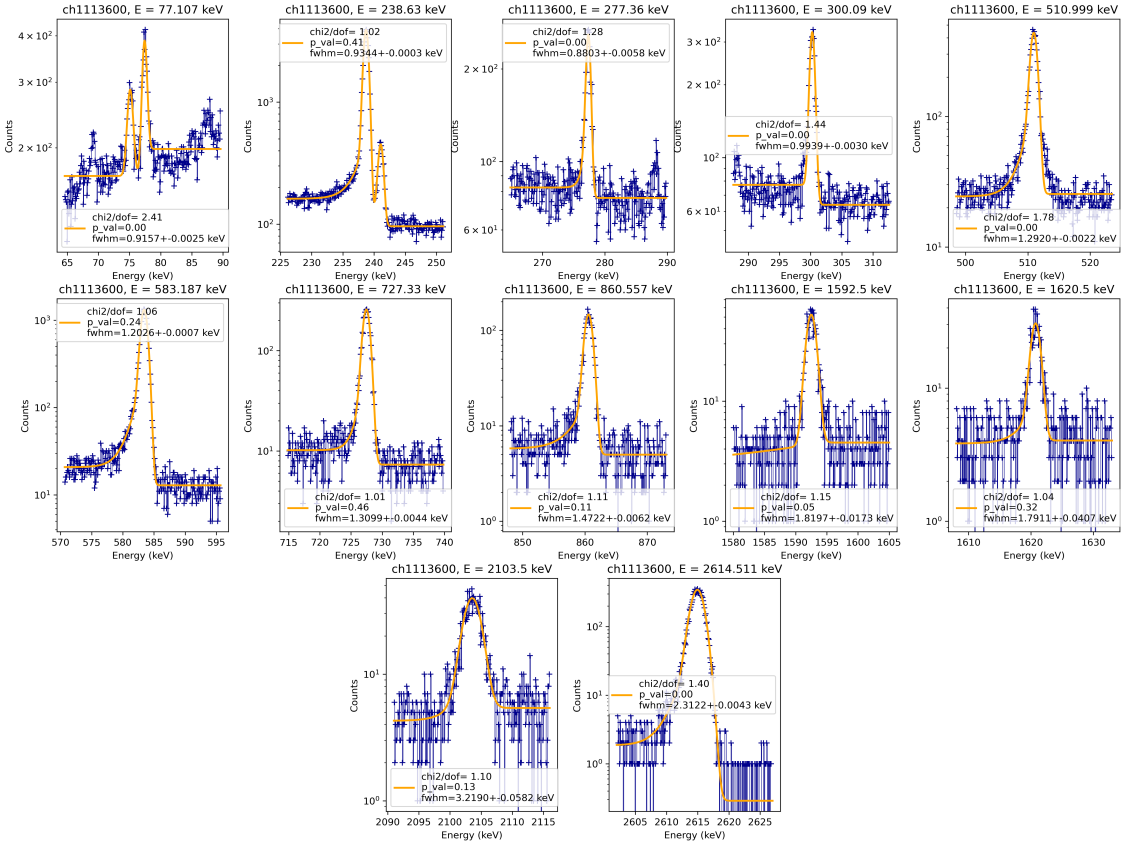

Figure 18: Fitted energy peaks for detector B00000C. Note that for the double peaks e.g. 74.815/77.107 keV and 238.63/240.99 keV, only the FWHM of the peak with the greater intensity was implemented. In this case, the FWHM from 77.107 and 238.63 keV.

Next, the resolutions on the calibrated energy E were then fitted with the function

$$\sigma(E) = \sqrt{a + bE} \tag{6}$$

where a and b are fit parameters. The former accounts for the contributions from electronic noise, while the latter accounts for statistical fluctuations in the number of charge carriers [32]. The FWHM and the corresponding uncertainties of each peak are extracted and via Eq. 6 to model the resolution as a function of energy.

The resulting resolution curve is shown in Fig. 19. Interpolating the resolution at $Q_{\beta\beta}$ yields a result of **(2.03±0.05) keV**. It is worth noting that the SEP (red dot in Fig. 19) is excluded from the fit of the detector's resolution because of the Doppler effect. The motion of the electron–positron pair prior to annihilation is the source of Doppler broadening of the resulting 511-keV annihilation gamma rays [38]. The Doppler effect could add 2 keV to other uncertainties contributing to the width of spectrum peaks [39]. The grey dashed lines indicate the spread within one standard deviation.

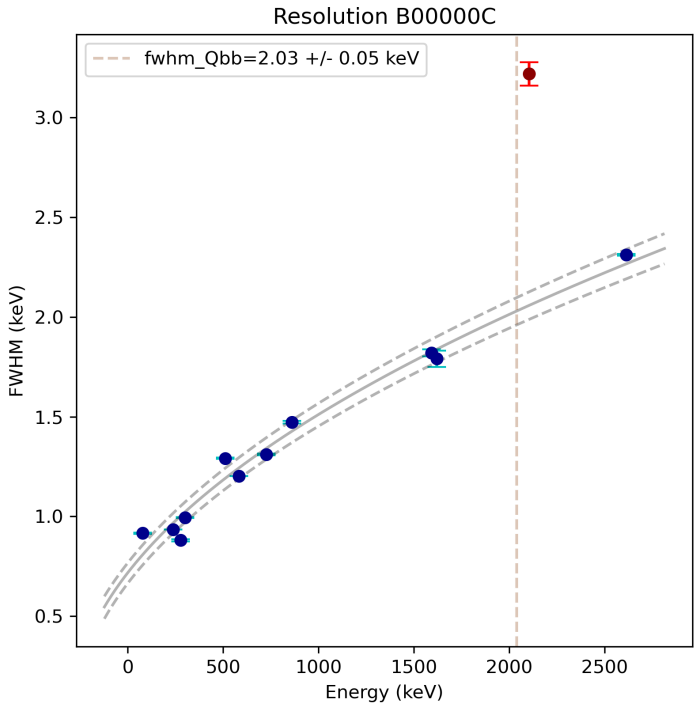

Figure 19: Resolution curve of the detector B00000C with the corresponding uncertainties on the FWHM of the fits. The intersection of the vertical dashed line with the grey continuous line indicates the resolution of the detector at $Q_{\beta\beta}$.

This procedure was applied to all 12 detectors, which identified the 77 keV peak. The resolution of all these detectors before and after implementing the low energy peaks are shown in Fig. 20. It was observed that the uncertainties on the new resolution values including the low energy peaks are clearly higher for most detectors. A probable explanation lies in the fit functions used in this work. In the standard LEGEND-200 calibration, peak fitting is well taken care of for different detectors by

selecting optimal peak-fit functions for individual detectors, whereas in this work, a universal peak-fit function as mentioned in the beginning of Sec. 4 was applied to all energy peaks. Also, to ensure a clear comparison between resolution data with and without the implementation of the 74.815/77.107 keV peaks, peak-fit results for all energy peaks were included even for fit results with small p-values. This opened the possibility for bad fits with large uncertainties to influence the resolution and its uncertainty. In the majority of the detectors, the resolution remained constant with respect to the previous value. Looking at the detector type, it can be seen that the resolution for both, before and after including low energy peaks in the resolution fit function, is best for the BEGe detectors. For this detector type, no significant deteriorations are observed in the resolution, even some light improvements were achieved, such as B00061A and B00089D in period 07, run 008 as well as B00061C and B00002C in period 08, run 002. For the previously introduced detector, B00000C, the resolution remained constant for both investigated calibration runs. The biggest mismatches in resolution values before and after implementation of low energy peaks were obtained by the ICPC detectors. A posterior discussion with representatives from the LEGEND-200 experiment confirmed that these outliers resulted from the malfunction of several ICPC detectors, including V05261A, V01389A and V05612B.

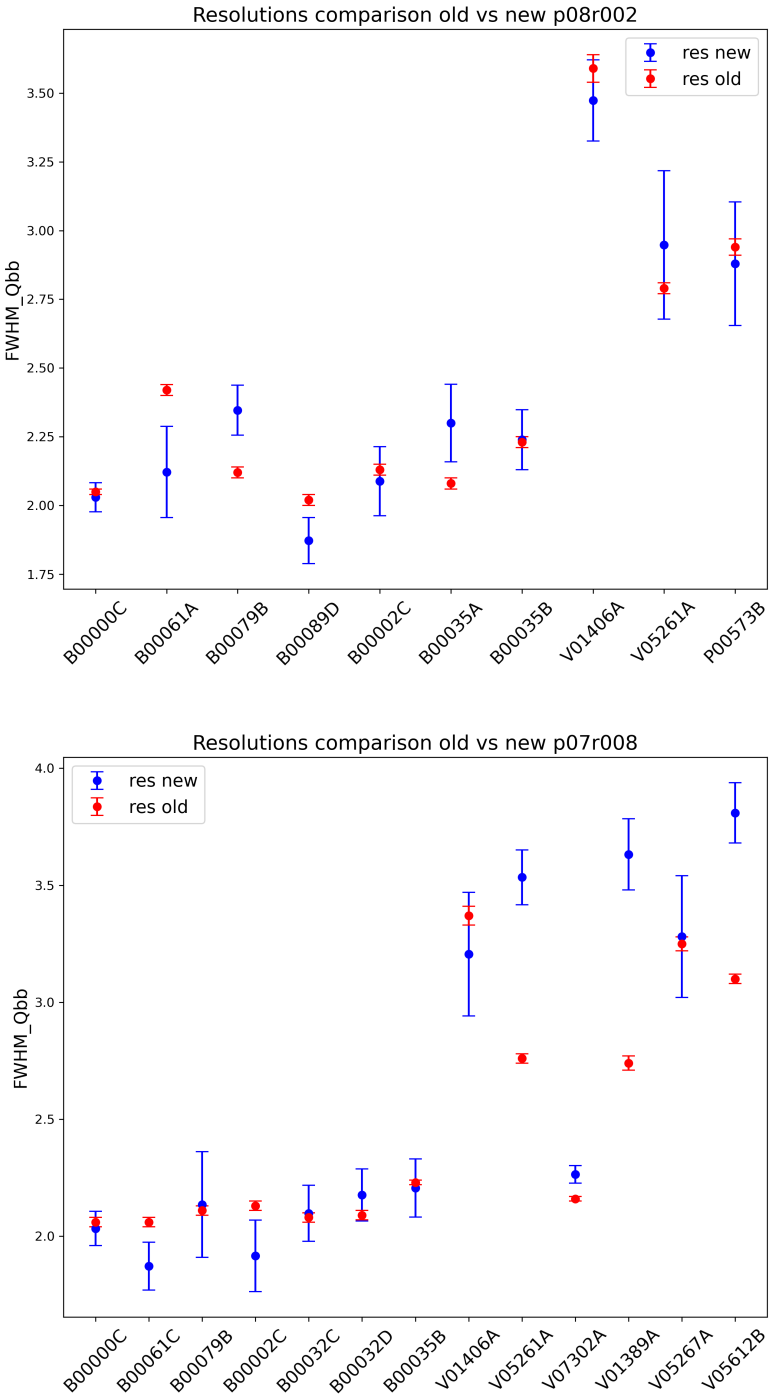

Figure 20: Old resolutions at $Q_{\beta\beta}$ in red and new resolutions at $Q_{\beta\beta}$ in blue. "Old" resolutions refer to the resolution obtained from the calibration with the seven peaks used in LEGEND-200, whereas "new" resolutions indicates the results obtained from the calibration with the low-energy peaks. All employed energy peaks are summarized in Tab. 2. Top: period 08 / run 002. Bottom: period 07 / run 008. LEGEND-200 data version: v1.0.0.

5 Conclusion and Outlook

In this work, the calibration data of the LEGEND-200 experiment was analyzed. The goal was to explore new energy peaks in detectors' energy spectra, useful for calibration in lower energy regions not used in the current LEGEND-200 standard calibration procedure. Three studies were conducted with LEGEND-200 calibration data.

The investigation commenced with an examination of coincident events in nearby detectors. The anticipation was that such occurrences would manifest as discernible hotspots within a 2D histogram, if there were preferred combinations in the deposited energy combinations. However, no clear hotspot indicating coincident events was observed due to the low cross section for Compton scattering in the investigated energy range. Instead, distinct vertical and horizontal lines emerged within the histogram, unequivocally indicative of complete energy deposition attributable to individual photons in a singular detector. To ascertain a precise estimation of energy, scrutiny extended to the one-dimensional energy spectrum, subsequently compared against established values within relevant literature. This analysis revealed two energy peaks centered at 74.815 keV and 77.107 keV, consistent with emissions originating from the ^{212}Pb isotope. These results were expected, as for energies between 50 keV and 230 keV, the cross section for the photoelectric effect dominates over the one for Compton scattering by up to two orders of magnitude in low energies.

Subsequently, an energy correlation analysis was undertaken, aimed at identifying an anti-diagonal correlation line within the two-dimensional histogram. This analysis was conducted over the whole energy range between 100 keV and 2.6 MeV, revealing the presence of an anti-diagonal correlation line for both the ^{208}Tl FEP at 2614.5 keV and the 583 keV peak, indicative of partial energy depositions occurring in proximate detectors. Due to the 50 keV threshold, the study was limited to γ rays with a total energy superior to 100 keV. Therefore, the two 74.815/77.107 keV lines are not suitable.

In the last study, the low-energy peaks were implemented in the usual calibration procedure. The goal of this investigation was to probe the potential of including the 74.815 and 77.107 keV energy peaks into the standard calibration procedure, and how this implementation would affect the resolution of the HPGe detectors. The probability of identifying these two energy peaks in detectors' energy spectra

is about 10% for two randomly selected calibration runs. In most of the considered detectors, the resolution stayed constant or worsened.

For future studies the regime of 50 keV to 583 keV in the LEGEND-200 experiment will remain important, as, besides the search for the $0\nu\beta\beta$ decay, there are many other BSM processes in lower energies, which are explored by the LEGEND collaboration. Therefore, a precise calibration of the HPGe detectors is crucial. A prospective study includes the examination of the efficacy of linear versus quadratic calibration curves. This analysis would involve investigating the residuals of the energy values for all detectors and determining the preferred degree for the polynomial fit with smaller residuals. The results gleaned from this investigation could then inform the calibration protocols of the LEGEND-200 experiment accordingly.

Appendix A

2D histograms

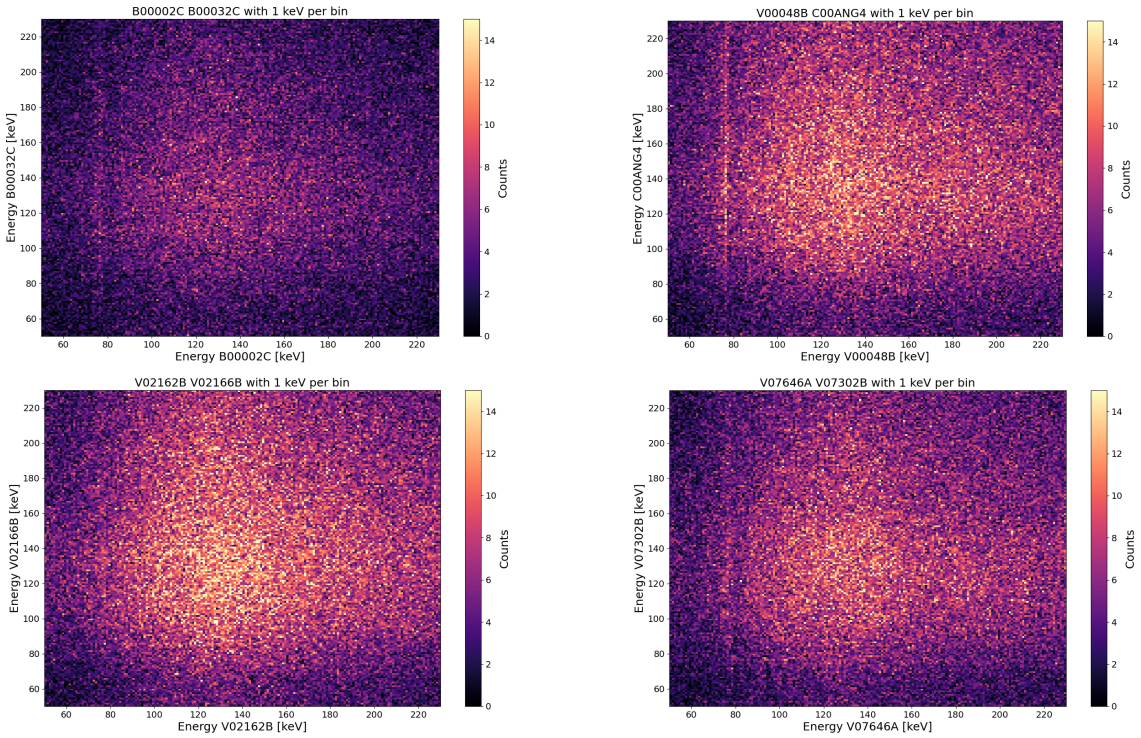

Figure 21: Further examples of 2D histograms for different detector combinations. Top left: vertical line visible for detector combination B00002C and B00032C. Top right: vertical line visible for detector combination V00048B and C00ANG4. Bottom left: No signatures for detector combination V02162B and V02166B. Bottom right: faint vertical and horizontal line visible for detector combination V07646A and V07302B.

Appendix B

Period 07 run 008		
Detector	Mass [g]	String
B00000C*	815	4
B00061C*	634	4
B00079C	812	4
V01406A	1382.6	4
V05261A	1797	8
V07302A	1803	8
B00002C*	788	10
B00032C	743	10
B00032D	720	10
B00035B*	810	10
V01240A*	2100	10
V01389A	2093.1	10
V05267A	2183	10
V05612B	2092	10

Period 08 run 002		
Detector	Mass [g]	String
B00000C*	815	4
B00061A	731	4
B00079B	736	4
V01406A	1382.6	4
B00089D	526	8
V05261A	1797	8
B00002C	788	10
B00035A	768	10
B00035B*	810	10
P00573B	1067.8	11

Table 3: List of detectors that detected the 77.107 keV peak, with each detector's mass and string in the periods/runs of p07/r008 and p08/r002.
*74.815 keV peak also detected.

List of abbreviations

$0\nu\beta\beta$, neutrinoless $\beta\beta$ decay
$2\nu\beta\beta$, two-neutrino $\beta\beta$ decay
ADC, analog-to-digital converter
BEGe, broad-energy germanium detector
BSM, beyond Standard Model
Coax, coaxially shaped detector
DEP, double escape peak
FEP, full energy peak
FWHM, full width at half maximum
GERDA, Germanium Detector Array
HPGe, high-purity germanium detector
ICPC, inverted coaxial point-contact detector
LAr, liquid argon
LEGEND, Large Enriched Germanium Experiment for Neutrinoless $\beta\beta$ Decay
LNGS, Laboratori Nazionali del Gran Sasso
MJD, Majorana Demonstrator
MSE, multi-site event
PMT, photo-multiplier tube
PPC, p-type point-contact detector
PSD, pulse shape discrimination
PTFE, polytetrafluoroethylene
ROI, region of interest
SEP, single escape peak
SIS, source insertion system
SM, Standard Model
SNR, signal-to-noise ratio
SSE, single-site event

Acknowledgments

First, I would like to thank my extraordinary supervisor, Dr. Pin-Jung Chiu, for her incredible support during my entire journey working on this thesis. Without her, it would have been impossible for me to carry out this project. You showed me that coding can indeed be very fun, even for someone like me without much experience or talent in this field, and that by working hard, anything is possible. Next, I want to thank Prof. Laura Baudis for making all of this possible and giving me the opportunity to actively participate in a fantastic research group. I also want to give special thanks to Francesco, Gabriela, Thomas, Christian and Marta for providing me with very valuable inputs, useful data for this work, and for taking the time to carefully read through this thesis. Last but not least, I want to extend my thanks to the entire Baudis group. You welcomed me with open arms, and made me feel very comfortable. Even though I have only been here for a few months, it felt like I had been a group member for years. Thank you for all the amusing moments during lunch breaks, runs in the forest, and meetings. The experience of working in this group is something I will never forget.

References

[1] A. De Angelis and M. Pimenta. *Introduction to Astroparticle Physics*. Springer Cham, 2018. ISBN: 978-3-319-78180-8.

[2] R. Oerter. *The theory of almost everything: The standard model, the unsung triumph of modern physics*. Penguin, 2006.

[3] R. L. Workman et al. "Review of Particle Physics". In: *PTEP* 2022 (2022), p. 083C01. DOI: 10.1093/ptep/ptac097.

[4] J. Kónya and N. M. Nagy. *Nuclear and radiochemistry*. Elsevier, 2018.

[5] A. Giuliani, A. Poves, et al. "Neutrinoless double-beta decay". In: *Advances in High Energy Physics* 2012 (2012).

[6] M. Goeppert-Mayer. "Double Beta-Disintegration". In: *Phys. Rev.* 48 (6 Sept. 1935), pp. 512–516. DOI: 10.1103/PhysRev.48.512. URL: https://link.aps.org/doi/10.1103/PhysRev.48.512.

[7] E. Majorana. "Teoria simmetrica dell'elettrone e del positrone". it. In: *Il Nuovo Cimento* 14.4 (Apr. 1937), pp. 171–184.

[8] M. Agostini et al. "Search of Neutrinoless Double Beta Decay with the GERDA Experiment". In: *Nuclear and Particle Physics Proceedings* 273–275 (Apr. 2016), pp. 1876–1882. ISSN: 2405-6014. DOI: 10.1016/j.nuclphysbps.2015.09.303.

[9] V. A. Rubakov and M. E. Shaposhnikov. "Electroweak baryon number non-conservation in the early Universe and in high-energy collisions". In: *Phys.–Usp.* 39.5 (May 1996), pp. 461–502.

[10] A. D. Sakharov. "Violation of CP Invariance, C asymmetry, and baryon asymmetry of the universe". In: *Pisma Zh. Eksp. Teor. Fiz.* 5 (1967), pp. 32–35. DOI: 10.1070/PU1991v034n05ABEH002497.

[11] M. Agostini et al. "Final Results of GERDA on the Search for Neutrinoless Double-β Decay". In: *Phys. Rev. Lett.* 125 (25 Dec. 2020), p. 252502. DOI: 10.1103/PhysRevLett.125.252502. URL: https://link.aps.org/doi/10.1103/PhysRevLett.125.252502.

[12] F. Edzards. "The Future of Neutrinoless Double Beta Decay Searches with Germanium Detectors". In: *Journal of Physics: Conference Series* 1690 (Dec. 2020), p. 012180. DOI: 10.1088/1742-6596/1690/1/012180.

[13] N. Abgrall et al. "The MAJORANA DEMONSTRATOR readout electronics system". In: *Journal of Instrumentation* 17.05 (May 2022), T05003. ISSN: 1748-0221. DOI: 10.1088/1748-0221/17/05/t05003. URL: http://dx.doi.org/10.1088/1748-0221/17/05/T05003.

[14] N. Abgrall et al. "The MAJORANA DEMONSTRATOR radioassay program". In: *Nuclear Instruments and Methods in Physics Research Section A: Accelerators, Spectrometers, Detectors and Associated Equipment* 828 (Aug. 2016), pp. 22–36. ISSN: 0168-9002. DOI: 10.1016/j.nima.2016.04.070. URL: http://dx.doi.org/10.1016/j.nima.2016.04.070.

[15] I. J. Arnquist et al. "Final Result of the MAJORANA DEMONSTRATOR's Search for Neutrinoless Double-β Decay in ^{76}Ge". In: *Phys. Rev. Lett.* 130 (6 Feb. 2023), p. 062501. DOI: 10.1103/PhysRevLett.130.062501. URL: https://link.aps.org/doi/10.1103/PhysRevLett.130.062501.

[16] G. Bellini et al. "Cosmic-muon flux and annual modulation in Borexino at 3800 m water-equivalent depth". In: *Journal of Cosmology and Astroparticle Physics* 2012.05 (May 2012), pp. 015–015. ISSN: 1475-7516. DOI: 10.1088/1475-7516/2012/05/015. URL: http://dx.doi.org/10.1088/1475-7516/2012/05/015.

[17] Yannick Müller. "Calibration of the LEGEND-200 Experiment to Search for Neutrinoless Double Beta Decay and Searches for Signatures of New Physics with the GERDA Experiment". PhD thesis. Universität Zürich, 2023.

[18] Gabriela Rodrigues Araujo. "Advancing Neutrinoless Double Beta Decay Search with LEGEND and MONUMENT and Exploring Passive Neutrino Detectors with PALEOCCENE". PhD thesis. Universität Zürich, 2023.

[19] L. Collaboration et al. *LEGEND-1000 Preconceptual Design Report*. 2021. arXiv: 2107.11462 [physics.ins-det].

[20] A. J. Zsigmond, L. Collaboration, et al. "LEGEND: The future of neutrinoless double-beta decay search with germanium detectors". In: *Journal of Physics: Conference Series*. Vol. 1468. 1. IOP Publishing. 2020, p. 012111.

[21] B. J. Mount, M. Redshaw, and E. G. Myers. "Double-β-decay Q values of ^{74}Se and ^{76}Ge". In: *Phys. Rev. C* 81 (3 Mar. 2010), p. 032501. DOI: 10.1103/PhysRevC.81.032501. URL: https://link.aps.org/doi/10.1103/PhysRevC.81.032501.

[22] N. Abgrall et al. "The processing of enriched germanium for the MAJORANA DEMONSTRATOR and and R&D for a Possible Future Ton-Scale Ge-76 Double-Beta Decay Experiment". In: *Nuclear Instruments and Methods in Physics Research Section A: Accelerators, Spectrometers, Detectors and Associated Equipment* 877 (Jan. 2018), pp. 314–322. ISSN: 0168-9002. DOI: 10.1016/j.nima.2017.09.036. URL: http://dx.doi.org/10.1016/j.nima.2017.09.036.

[23] G. collaboration et al. "Limits on uranium and thorium bulk content in GERDA Phase I detectors". In: *Astroparticle Physics* 91 (May 2017), pp. 15–21. ISSN: 0927-6505. DOI: 10.1016/j.astropartphys.2017.03.003. URL: http://dx.doi.org/10.1016/j.astropartphys.2017.03.003.

[24] V. D'Andrea et al. "Neutrinoless Double Beta Decay with Germanium Detectors: 10^{26} yr and Beyond". In: *Universe* 7.9 (Sept. 2021), p. 341. ISSN: 2218-1997. DOI: 10.3390/universe7090341. URL: http://dx.doi.org/10.3390/universe7090341.

[25] M. Agostini et al. "Final Results of GERDA on the Two-Neutrino Double-β Decay Half-Life of ^{76}Ge". In: *Phys. Rev. Lett.* 131 (14 Oct. 2023), p. 142501. DOI: 10.1103/PhysRevLett.131.142501. URL: https://link.aps.org/doi/10.1103/PhysRevLett.131.142501.

[26] Luigi Pertoldi. "Search for new physics with two-neutrino double-beta decay in GERDA data". PhD thesis. Universita degli Studi di Padova, 2021.

[27] F. Edzards et al. "Surface Characterization of P-Type Point Contact Germanium Detectors". In: *Particles* 4.4 (Oct. 2021), pp. 489–511. ISSN: 2571-712X. DOI: 10.3390/particles4040036. URL: http://dx.doi.org/10.3390/particles4040036.

[28] M. Agostini et al. "Characterization of inverted coaxial ^{76}Ge detectors in GERDA for future double-β decay experiments". In: *The European Physical Journal C* 81.6 (June 2021). ISSN: 1434-6052. DOI: 10.1140/epjc/s10052-021-09184-8. URL: http://dx.doi.org/10.1140/epjc/s10052-021-09184-8.

[29] A. Domula et al. "Pulse shape discrimination performance of inverted coaxial Ge detectors". In: *Nuclear Instruments and Methods in Physics Research Section A: Accelerators, Spectrometers, Detectors and Associated Equipment* 891

(May 2018), pp. 106–110. ISSN: 0168-9002. DOI: 10.1016/j.nima.2018.02.056. URL: http://dx.doi.org/10.1016/j.nima.2018.02.056.

[30] L. Baudis et al. "Calibration sources for the LEGEND-200 experiment". In: *Journal of Instrumentation* 18.02 (Feb. 2023), P02001. ISSN: 1748-0221. DOI: 10.1088/1748-0221/18/02/p02001. URL: http://dx.doi.org/10.1088/1748-0221/18/02/P02001.

[31] N. Abgrall et al. "ADC Nonlinearity Correction for the MAJORANA DEMONSTRATOR". In: *IEEE Transactions on Nuclear Science* 68.3 (2021), pp. 359–367. DOI: 10.1109/TNS.2020.3043671.

[32] M. Agostini et al. "Calibration of the GERDA experiment". In: *The European Physical Journal C* 81.8 (Aug. 2021). ISSN: 1434-6052. DOI: 10.1140/epjc/s10052-021-09403-2. URL: http://dx.doi.org/10.1140/epjc/s10052-021-09403-2.

[33] N. Abgrall et al. "The MAJORANA DEMONSTRATOR calibration system". In: *Nuclear Instruments and Methods in Physics Research Section A: Accelerators, Spectrometers, Detectors and Associated Equipment* 872 (Nov. 2017), pp. 16–22. ISSN: 0168-9002. DOI: 10.1016/j.nima.2017.08.005. URL: http://dx.doi.org/10.1016/j.nima.2017.08.005.

[34] National Institute of Standards and Technology Standard Reference Data Program, U.S. Department of Energy. *XCOM: Photon Cross Sections Database*. https://physics.nist.gov/PhysRefData/Xcom/html/xcom1.html. Accessed: 23-04-2024.

[35] National Nuclear Data Center (NNDC). *Nudat 3.0*. https://www.nndc.bnl.gov/nudat3/. Accessed: 06-03-2024.

[36] S.Y.F. Chu, L.P. Ekström, R.B. Firestone. *Table of Radioactive Isotopes*. http://nucleardata.nuclear.lu.se/nucleardata/toi/. Accessed: 15-04-2024.

[37] I. Bikit et al. "Coincidence Techniques in Gamma-ray Spectroscopy". In: *Physics Procedia* 31 (2012), pp. 84–92. ISSN: 1875-3892. DOI: 10.1016/j.phpro.2012.04.012.

[38] R. L. Coldwell and G. P. Lasche. "Experimental measurements of Doppler broadening of escape peaks in HPGe detectors". In: *Journal of Radioanalytical and Nuclear Chemistry* 307.3 (2016), pp. 2509–2512.

[39] G. Gilmore. *Practical gamma-ray spectroscopy*. John Wiley & Sons, 2008.